Electrophysiological Studies on Cerebellar Synaptic Transmission in P/Q-type Ca^{2+} Channel Mutant Mice

Kaori Matsushita

DOCTOR OF PHILOSOPHY

Department of Physiological Sciences
School of Life Science
The Graduate University for Advanced Studies

2001

CONTENTS

ABSTRACT

Homozygous ataxic mice, tottering (*tg*) and rolling Nagoya (tg^{rol}), have mutations in the P/Q-type Ca^{2+} channel α_{1A} subunit gene. The location of the mutations and the neurological phenotypes are known, but the mechanisms how the mutations cause the symptoms and how the different mutations lead to various onset and severity have remained unsolved. Here we compared fundamental properties of excitatory synaptic transmission in the cerebellum and its sensitivity to subtype-specific Ca^{2+} channel blockers among wild-type control, *tg*, and tg^{rol} mice. The amplitude of excitatory postsynaptic current (EPSC) of the parallel fiber-Purkinje cell (PF-PC) synapses was considerably reduced in ataxic tg^{rol}. Whereas the PF-PC EPSC amplitude was only mildly decreased in non-ataxic *tg* mice, the PF-PC EPSC was drastically diminished in ataxic *tg* mice of P28-35. In contrast, the EPSC amplitude of the climbing fiber-Purkinje cell (CF-PC) synapses was preserved in *tg*, and it was even increased in tg^{rol}. CF-PC EPSC was more dependent on the N- and R-type Ca^{2+} channels in mutant mice, suggesting that such compensatory mechanisms contribute to maintain the CF-PC synaptic transmission virtually intact. These results indicate that the impairment of the PF-PC synaptic transmission well correlates with manifestation of ataxia, and that different mutations of the P/Q-type Ca^{2+} channel not only cause the primary effect of various severity but also lead to diverse secondary effects, which include up-regulation of other Ca^{2+} channel subtypes and enhancement of sensitivity of postsynaptic glutamate receptors.

INTRODUCTION

Ca^{2+} controls diverse cellular processes, which include neurotransmitter release and other forms of secretion, gene expression, and cell proliferation (Tsien and Tsien, 1990; Ghosh and Greenberg, 1995). To evoke these cellular responses, Ca^{2+} influx across the plasma membrane makes a major contribution to augmenting the cytosolic Ca^{2+} concentration. Multiple voltage-gated Ca^{2+} channel types, including five high-threshold types (L, N, P, Q, and R) and the low-threshold T-type, form major Ca^{2+} entry pathways in neurons (Catterall, 2000). Several of these types are colocalized in a single neuron and are assumed to contribute to fine tuning of neuronal activity, because each type is differently modulated. Although the critical role of Ca^{2+} channels, particularly the P/Q- and N-types, for neurotransmitter release has been well established (Hirning et al., 1988; Turner et al., 1992; Takahashi and Momiyama, 1993; Artalejo et al., 1994; Regehr and Mintz, 1994), the role of Ca^{2+} channels in integration of signals or synaptic plasticity has been poorly understood.

Voltage-gated Ca^{2+} channels are composed of the main pore-forming α_1 subunit, encoded by a family of genes, and the accessory α_2/δ, β and γ subunits (Catterall, 2000). The α_{1A} subunit was originally characterized as a high-voltage-activated Ca^{2+} channel that is resistant to blockade by the N-type-selective inhibitor ω-conotoxin GVIA (ω-CgTx) or the L-type inhibitor dihydropyridines (Mori et al., 1991). It is now accepted that the P- and Q-types, which differ in sensitivity to ω-agatoxin-IVA (ω-Aga-IVA) and inactivation kinetics (Llinás et al., 1989; Regan et al., 1991; Mintz et al., 1992; Zhang et al., 1993), are produced from the single α_{1A} gene by alternative splicing (Mori et al., 1991; Sather et al., 1993; Bourinet et al., 1999) and/or through association with different

isoforms of accessory subunits (Stea et al., 1994), although the mechanism by which different phenotypes are produced has not been fully explained yet (Bourinet et al., 1999).

Molecular genetic analyses have identified that mutations of the gene encoding the Ca^{2+} channel α_{1A} subunit are associated with cerebellar ataxia and other forms of neurological disorders in human (Ophoff et al., 1996). To elucidate the pathophysiology of these human genetic channelopathies and to develop methods for treatment, spontaneous mouse mutants of the α_{1A} subunit gene are useful models. Recently, the well established mouse models of hereditary cerebellar ataxia, which include tottering (*tg*) (Green and Sidman, 1962), rolling (tg^{rol}) (Oda, 1973), and leaner (tg^{la}) (Sidman et al., 1965) were found to result from mutations of the Ca^{2+} channel α_{1A} subunit gene (Fletcher et al., 1996; Mori et al., 2000). The *tg* mutation is located in the extracellular region close to the pore-forming P-region of the second repeat (Fletcher et al., 1996). The tg^{rol} mutation is a single nucleotide alteration leading to the charge-neutralizing arginine to glycine substitution in the voltage-sensing S4 segment (Stühmer et al., 1989) of the third repeat (Mori et al., 2000). The tg^{rol} mutation causes not only a reduction in current amplitude but also a positive shift and reduction of slope of voltage-dependence of activation, in both native acutely dissociated Purkinje cells and culture cells recombinantly expressing the mutant P/Q type channel. The tg^{la} mutation is a single-base pair substitution in a splice donor consensus sequence, which results in altered C-terminal sequences (Fletcher et al., 1996). Homozygous tg^{la} mutant mice are severely ataxic (Herrup and Wilczynski, 1982).

Cerebellar ataxia has been identified as the common abnormality among the α_{1A}

mutant mice. Severity of cerebellar ataxia, however, differs significantly; *tg* shows the mildest ataxia, whereas the symptom of tg^{la} is the severest . Previous studies to compare *tg*, tg^{la} (Wakamori et al., 1998) and tg^{rnl} (Mori et al., 2000) suggested that severity of the cerebellar defect is somewhat correlated with the degree of deviation in P/Q-type channel properties of Purkinje cells. But the mechanism how the abnormalities of the channel function lead to ataxia has remained unsolved.

Neuronal circuits of the cerebellar cortex have been well characterized (Llinás and Walton, 1998). The cerebellar cortex receives inputs from two main sources, mossy fibers and climbing fibers, and only one type of cells, Purkinje neurons, are responsible for output. The mossy fiber system originates from a variety of sources and provides, through granule cells, a numerically impressive innervation (up to 150,000 parallel-fiber inputs) on the terminal regions of Purkinje cell dendrites. In contrast, one climbing fiber originating in the inferior olive innervates the apical dendrite of each Purkinje cell. Channel dysfunction, therefore, may affect the cerebellar excitatory synaptic inputs, that may consequently cause dysfunction of cerebellar circuits. Thus, studying these mutant mice could provide important clues in understanding not only the roles of Ca^{2+} channels in integration of neuronal signaling but also pathophysiology of the human genetic diseases. In this study, I studied basic properties of excitatory synaptic transmission in the parallel fiber-Purkinje cell (PF-PC) and climbing fiber-Purkinje cell (CF-PC) synapses of wild-type control (wt), *tg* and tg^{rnl}. The present data demonstrated that the different mutations in one gene can cause distinct dysfunction and secondary changes in the neural circuit, which underlie the common symptom of cerebellar ataxia.

Experimental Procedures

Animals

The C57BL/6J-*tg* strain of *tg* mice was introduced from the Jackson Laboratory (Bar Harbor, MA). The tg^{rol} mice were provided by Dr. S. Oda (Nagoya University). These mice were provided with a commercial diet (CE-2, Nihon Clea, Tokyo, Japan) and water *ad libitum* under conventional conditions with controlled temperature, humidity, and lighting (22 ± 2°C, 55 ± 5%, and 12-h light-dark cycle with lights on at 07:00). The strains were maintained and propagated by mating between heterozygous mice in the Center for Experimental Animals, Okazaki National Research Institutes.

PCR-RFLP genotyping

Genotyping of *tg* mice was performed using PCR-restriction fragment length polymorphism (PCR-RFLP). A PCR fragment was obtained using a pair of primers, 5'-GGAAACCAGAAGCTGAACCA-3' (sense) and 5'-GAAATGGAGGAATTCAGGG-3' (anti-sense) and genomic DNA as a template. Digestion of the fragment with *Aci*I yielded the following fragments: 295 bp in *tg/tg*, 127 and 168 bp in +/+, and 127, 168 and 295 bp in *tg*/+ (Wakamori et al, 1998). Since tg^{rol}/tg^{rol} mice exhibit overt ataxia at two weeks of age, it was not necessary to conduct genotyping using the molecular biological methods.

Slice preparation

Mice were killed by decapitation under halothane general anesthesia, in accordance with the institutional guideline for animal experiments. Brains were removed from wt, *tg*,

and tg^{rol} mice at postnatal days 14-20 (P14-20) and wt and *tg* at P28-35 and cooled in ice-cold saline (described below). Parasagittal 250-μm-thick slices were cut from the cerebellar vermis with a vibratome (DTK-1000; Dosaka, Kyoto, Japan). Slices were kept at room temprature for 1 hour after slicing in the artificial cerebrospinal fluid (ACSF) containing (in mM): 125 NaCl, 25 $NaHCO_3$, 25 glucose, 2.5 KCl, 1.25 NaH_2PO_4, 2 $CaCl_2$, and 1 $MgCl_2$, bubbled with carbogene (95% O_2 and 5% CO_2).

Electrophysiology

After 1-hour incubation at room temperature, slices were transferred to a recording chamber and perfused with ACSF. Bicuculline (10 μM) was always present in the saline to block spontaneous inhibitory postsynaptic currents. A whole-cell voltage-clamp recording was made from Purkinje cells, which were visually identified using an upright microscope (Axioskop FS, Carl Zeiss, Jena, Germany) equipped with a ×60 water immersion objective (Olympus Optical, Tokyo, Japan) and an infrared differential interference contrast video system (C2400-07, Hamamatsu Photonics, Hamamatsu, Japan) (Edwards et al., 1989; Llano et al., 1991). Patch pipettes were made from borosilicate capillaries (2.0 mm outer diameter and 1.0 mm inner diameter; Hilgenberg, Malsfeld, Germany). The resistance of patch pipettes was 3-5 MΩ when filled with an intracellular solution, which contained (mM): 100 Cs-gluconate, 34.5 CsCl, 4 NaCl, 10 HEPES, 4 Mg-ATP, 0.3 Na-GTP, 10 EGTA (adjusted to pH 7.3 with CsOH). QX-314 (final 5 mM) was added to prevent Na^+ spike generation. The liquid junction potential was measured to be approximately –8 mV, but was not corrected. Excitatory postsynaptic currents (EPSCs) were recorded with an EPC7 patch-clamp amplifier

(List-Medical-Electronics, Darmstadt, Germany). Stimulation and data acquisition were performed using the PULSE program (version 7.5, HEKA Elektronik, Lambrecht, Germany). The signals were filtered at 3 kHz and digitized at 20 kHz. The experiments were performed at a bath temperature of 32°C.

Somatic whole-cell voltage recording in the current-clamp mode was made with 4-8 MΩ patch pipettes using the EPC-7 amplifier. The patch pipettes were filled with the following internal solution, containing (in mM): 135 K-gluconate, 20 KCl, 2 $MgCl_2$, 2 Na_2ATP, 0.3 NaGTP, 0.2-0.5 EGTA, and 10 HEPES (pH was adjusted to 7.3 with KOH). Patch pipette resistance was 5-10 MΩ. After establishing the whole cell configuration, the membrane potential was maintained at –70 mV by injecting a constant current ranging between 50-250 pA. During the experiments, input resistance was periodically monitored by measuring the steady-state current evoked by 10 mV pulses in a Purkinje cell voltage-clamped at –70 mV. Cells were rejected if input resistance decreased below 80 MΩ. The signals were filtered at 3 kHz and digitized at 50 kHz. The experiments were performed at a bath temperature of 32°C.

Parallel fiber response

Parallel fiber-mediated EPSCs (PF-PC EPSCs) were evoked by electrical stimulation, using a bipolar electrode with a tip diameter of 13 μm made from a theta-shaped glass capillary (TGC200, Clark Electromedical Instruments, Reading, England) and filled with 1 M NaCl. Square pulses of 100 μs duration and amplitude ranging from 1.5 to 12 V were applied, while the stimulation glass pipette was moved within the visual field until the synaptic current was evoked with minimum stimulus intensity. The stimulation

pipette was usually placed at ~100 μm from the pial surface. The holding potential was adjusted in every experimental condition to make the driving force constant (70 mV) for inward currents. Evoked EPSC amplitude was compared among wt, *tg*, and tg^{rnl} at P14-20 or P28-35. In the three types of mice, the current-voltage (I-V) relationship was linear (data not shown).

Climbing fiber response

Climbing fiber-mediated EPSCs (CF-PC EPSCs) were evoked by electrical stimulation, using a bipolar electrode fabricated from a theta-shaped capillary. The glass pipette had a tip size of 10-13 μm, and was filled with 1 M NaCl. The pipette was placed in the granule cell layer at a distance of 50-100 μm from the Purkinje cell where EPSCs were measured. Square pulses (duration 100 μs, amplitude 1-10 V) were applied for focal stimulation. The holding potential was set in every experimental condition to make the driving force constant (20 mV) for inward currents. The evoked EPSC amplitudes were compared among wt, *tg*, and tg^{rnl} at P14-20 or P28-35.

Because the large size of CF-EPSCs and the extensive dendritic arbor of Purkinje cells make voltage clamp of these currents technically difficult, I adopted several strategies to optimize the quality of voltage-clamp and to minimize the errors involved. Firstly, P14-20 mice (mainly P17) were used, as at this age the Purkinje cell dendritic arbor is less extensive than in the adult, and CF innervation is located on the soma and proximal dendrites (Altman and McCrady, 1972). Secondly, the electrode resistance was minimized by using large electrodes (3-4 MΩ), combined with series resistance compensation (50-70%). Series resistance was monitored by measuring the transient

current evoked by 10 mV pulses in a Purkinje cell held at –70 mV. Cells were rejected if it increased above 20 MΩ. Thirdly, recordings were made at depolarized voltages so that the amplitudes of synaptic currents were reduced and voltage-gated currents inactivated.

We observed innervation of multiple climbing fibers only in few wt and *tg* Purkinje cells, but we observed multiple innervation more frequently in tg^{rol} Purkinje cells. In this study, we excluded Purkinje cells with multiple innervation from the analyses.

Miniature CF-EPSCs

For recording miniature CF-EPSCs, we used mouse brains from P14-20 and P28-35 wt, ataxic tg^{rol}, and *tg*. After establishing a stable condition for CF-EPSC measurements, we changed external solutions from ACSF to a Sr^{2+}-containing solution, which was composed of (in mM): 125 NaCl, 25 $NaHCO_3$, 25 glucose, 2.5 KCl, 1.25 NaH_2PO_4, 5 $SrCl_2$, and 5 $MgCl_2$ (Silver et a., 1998). The holding potential was –70 mV. CFs were stimulated at 0.2 Hz. Series resistance and reversal potential were measured periodically. We analyzed synaptic events larger than 40 pA in peak amplitude in a 100-ms time window starting 200 ms after stimulation. The decay phase of synaptic events was fitted with a single exponential.

Estimation of fractional contribution of Ca^{2+} channel subtypes

Nonlinear relationship between the presynaptic Ca^{2+} concentration and the postsynaptic current amplitude has been described at various synapses (Dodge and Rahamimoff, 1967). A small decrease in presynaptic Ca^{2+} entry can cause a large reduction in the

synaptic responses. The relative contributions of Ca^{2+} channel subtypes to EPSCs were estimated using a power relation, $I = (a + b + c)^m$, where I is normalized EPSC amplitude, and a, b, and c represent the fractions of presynaptic Ca^{2+} channel subtypes sensitive to ω-Aga-IVA and to ω-CgTx, and the fraction insensitive to both toxins, respectively. In other words, a, b, and c represent the respective fractions of the P/Q-, N-, and presumed R-type channel components. The value m is the power coefficient, and is assumed to be 3. The relative amplitude of postsynaptic currents remaining after application of ω-Aga-IVA (A), ω-CgTx (B), and both toxins (C) can be described as $A = (1-a)^m$, $B = (1-b)^m$, and $C = c^m$, respectively, using $a + b + c = 1$.

In addition, the Hill's equation, $I = A(a + b + c)^m / \{(a + b + c)^m + d^m\}$, is used for CF-EPSC (Momiyama and Koga, 2001), to take the saturation effect of Ca^{2+} binding sites into consideration, where A is a scaling facotor, d indicates a Ca^{2+} influx/concentration relative to $a + b + c$, at which CF-EPSC amplitude is half-maximal. The power factor of m=4 and the value of the relative half-saturation concentration of $d = 0.6$ were used to fulfill the condition $a + b + c = 1$.

To validate the estimates of contributions of Ca^{2+} channel subtypes, I examined the effect on PF-EPSC and CF-EPSC amplitudes of lowering the extracellular Ca^{2+} concentration from 2.0 mM (control) to 0.5 mM. The PF-EPSC and CF-EPSC amplitudes were normalized to the values with 2.0 mM Ca^{2+}, plotted against the extracellular Ca^{2+} concentration, and fit by the power relation or the Hill's equation.

Firing pattern evoked by CF stimulation

Complex spike of Purkinje cells was observed in current-clamp mode. Climbing fiber

stimulation induced typical complex spikes, which consisted of large EPSPs, one clear Na^+ spike followed by several spikelets with lower amplitudes.

Preparation of dissociated Purkinje cells

Purkinje cells were freshly dissociated from *tg*, *tg*^{rol}, and wt at P20-32. The procedure for obtaining dissociated cells from mice was similar to that described previously (Wakamori et al., 1993). Coronal slices (400-μm-thick) of cerebellum were prepared using the vibratome. After preincubation in Krebs' solution for 40 min at 31°C, the slices were digested: first in Krebs' solution containing 0.01% pronase (Calbiochem-Novabiochem, La Jolla, CA) for 25 min at 31°C and then in solution containing 0.01% thermolysin (type X; Sigma, St. Louis, MO) for 25 min at 31°C. The Krebs' solution used for preincubation and digestion contained the following (in mM): 124 NaCl, 5 KCl, 1.2 KH_2PO_4, 2.4 $CaCl_2$, 1.3 $MgSO_4$, 26 $NaHCO_3$, and 10 glucose. The solution was continuously oxygenated with 95% O_2 and 5% CO_2. Then Purkinje cell layer of the brain slices were punched out and dissociated mechanically by the use of fine glass pipettes having a tip diameter of 100-200 μm. Dissociated cells settled on tissue culture dishes (Primaria #3801, Nippon Becton Dickinson, Tokyo, Japan) within 30 min. Purkinje cells were identified by their large diameter and characteristic pear shape because of the stump of the apical dendrite. To make a sufficient space-clamp of the Purkinje cell body, Purkinje cells lacking most of dendrites were used throughout the present experiments.

Whole-cell recordings of dissociated Purkinje cells

Electrophysiological measurements were performed on acutely dissociated Purkinje cells. Currents were recorded at room temperature (22-25°C) using whole-cell mode of the patch-clamp technique with an Axopatch 200B patch-clamp amplifier (Axon Instruments, Foster City, CA). Patch pipettes were made from borosilicate glass capillaries (1.5 mm outer diameter and 0.87 mm inner diameter; Hilgenberg, Malsfeld, Germany). The patch electrodes were fire-polished. Pipette resistance ranged from 1 to 2 MΩ when filled with the pipette solutions described below. The series resistance was electronically compensated to >70%. Currents were sampled at 5 kHz after low-pass filtering at 1 kHz (-3 dB). Data were collected and analyzed using the pClamp 6.02 software (Axon Instruments). The external solution contained (in mM): 140 NaCl, 5 KCl, 2 $CaCl_2$, 10 glucose, 10 HEPES (adjusted to pH 7.4 with Tris). The pipette solution contained (in mM): 140 CsCl, 10 EGTA and pH adjusted to 7.2 with CsOH. Rapid application of drugs was made by a modified "Y-tube" method (Wakamori et al., 1998). The external solution surrounding a cell recorded was completely exchanged within 200 msec.

Data analysis and statistics

All values are given as means ± SE. Statistical comparison between normal and mutant mice or mutant channels was performed by *t*-test (*$p < 0.05$, **$p < 0.01$). Data analysis and fitting procedures were performed using IgorPro program (Wavemetrics, Lake Oswego, OR). To calculate the mean EPSC peak amplitude, 5-10 consecutive EPSCs were averaged from each experiment. The decaying phase of EPSCs was fit with a

single exponential.

Chemicals

Bicuculline, 6-cyano-7-nitroquinoxialine-2,3-dione (CNQX), and (±)-2-amino-5-phosphonopentanoic acid (APV) were obtained from Sigma (St. Louis, MO). Peptide toxins, ω-Aga-IVA and ω-CgTx, were obtained from Peptide Institute, Inc. (Japan, Osaka). Nifedipine was obtained from Alomone Labs (Jerusalem, Israel). All other chemicals were from Nacalai Tesque, Inc. (Kyoto, Japan.) or Wako Pure Chemical Industries, Ltd. (Osaka, Japan), unless otherwise specified. Stock solutions were made in distilled water or dimethylsulfoxide (for nifedipine, concentration of dimethylsulfoxide in the final solution, 0.1%). ω-CgTx and ω-Aga-IVA were coapplied with 1 mg/ml cytochrome C from horse heart (Nacalai Tesque) to prevent unspecific binding of the peptide toxins. Nifedipine was protected from light.

RESULTS

EPSCs at parallel fiber-Purkinje cell synapses in mutant mice

I recorded parallel fiber (PF)-mediated excitatory post-synaptic currents (EPSCs) (PF-EPSCs) in the whole-cell configuration from Purkinje cells in parasagittal cerebellar slices. The holding potential was adjusted to keep the driving force for inward currents constant (70 mV), and amplitudes of evoked PF-EPSCs were compared among wt, *tg*, and tg^{rol} at P14-20 or P28-35. A Purkinje cell receives inputs from a large number of parallel fibers, but focal stimulation in the molecular layer activates only a very limited number of parallel fibers. This fact made it difficult to compare PF-EPSC amplitudes in different slice preparations. To circumvent this problem, I stimulated parallel fibers at geometrically determined locations, and changed intensity of stimulation to obtain the current amplitude-stimulation intensity relationship.

PF stimulation evoked EPSCs, of which amplitudes increased almost linearly with increments of stimulation intensity in wt and mutant mice (Fig. 1). However, PF stimulation was consistently less effective to elicit PF-EPSCs in Purkinje cells of *tg* and ataxic tg^{rol} than wt Purkinje cells ($p < 0.05$) in the stimulation intensity range from 3 to 15 volts. Moreover, whereas PF-EPSCs of P14-20 *tg* mice, which do not have obvious ataxia, showed about 30% reduction in the amplitude, PF-EPSC amplitude exhibited a more dramatic reduction (~70%) in clearly ataxic *tg* mice at P28-35 (Fig. 2). The current-voltage (I-V) relationship for PF-EPSCs was linear in the three groups of mice (data not shown). These results demonstrate that PF-PC synaptic transmission is unambiguously impaired in *tg* and tg^{rol} mice, and that the degree of the amplitude reduction correlates with severity of the ataxic symptom.

Properties of PF-EPSCs

I measured the 10-90% rise time and the decay time constant of PF-EPSCs, obtained at the stimulus intensity of 10 V (Table 1). The decay phase was fitted with a single exponential function. Both parameters were not significantly different among wt, *tg*, and tg^{rol} mice, indicating that the mutations of the P/Q-type Ca^{2+} channel gene do not influence the kinetics of PF-EPSCs. PF-EPSCs could be blocked by 6-cyano-7-nitroquinoxialine-2,3-dione (CNQX, 10 μM), but were insensitive to an NMDA receptor antagonist (±)-2-amino-5-phosphonopentanoic acid (APV, 100 μM) (Fig. 3), showing that PF-EPSCs in Purkinje cells are mediated exclusively by non-NMDA receptors even in mutant mice, as previously reported in rat (Konnerth et al., 1990) and mouse (Aiba et al., 1994; Kano et al., 1995).

PF-EPSCs are known to exhibit a prominent paired-pulse facilitation (PPF). The PPF magnitudes in the tg^{rol} were significantly greater than wt or *tg* at 50 ms interpulse intervals (Figs 4 and 5). Because PPF is considered to reflect the amount of residual Ca^{2+} in presynaptic terminals (Zucker, 1989), this finding suggests that the amount of Ca^{2+} influx into tg^{rol} nerve terminal evoked by a single activation is too small for reliable synaptic transmission. In P28-35, however, the PPF magnitude in the ataxic *tg* showed no significant change compared to that of wt (Fig. 5B), suggesting that the altered PPF itself is not directly related to the ataxic symptom.

Ca^{2+} channel subtypes in PF-PC synapses

Previous studies of synaptic transmission at the rat cerebellar PF-PC synapse indicate that both N- and P/Q-type channels are involved in the release of neurotransmitter

(Mintz et al., 1995). Because the *tg* and *tg*^{rol} mutations decrease the P/Q-type Ca^{2+} channel currents at presynaptic terminals, less reliance of neurotransmitter release on the P/Q-type channel and more reliance on the N-type channel would be expected. To examine this prediction, I studied the effect on the PF-PC synaptic transmission in wt mice of the application of ω-Aga-IVA, a P/Q-type channel-selective blocker, and ω-CgTx, an N-type channel-selective blocker. Application of 0.2 μM ω-Aga-IVA to the wt slices almost abolished the synaptic currents in Purkinje neurons; on average, the PF-EPSCs were reduced by 90.9 ± 1.0% (n = 3; Fig. 6, Table 2). On the other hand, application of 3 μM ω-CgTx to the wild-type slices only partially blocked PF-EPSCs, reducing by 24.3 ± 4.5% (n = 3; Fig. 7). The remaining component after application of both toxins was 8.13 ± 1.2 %. Because the remaining component was not affect by nifedipine (10 μM), an L-type Ca^{2+} channel blocker, it likely corresponds to the R-type Ca^{2+} channel. Therefore, the wt PF terminals contain the P/Q-, N-, and presumed R-type Ca^{2+} channels, but the P/Q-type plays the predominant role.

When the same set of experiments was performed on *tg* and *tg*^{rol} mice (Figs 6 and 7, Table 2), application of ω-Aga-IVA (0.2 μM) caused a large decrease in PF-EPSC amplitude in *tg* (83.4 ± 2.3%, n = 3) and *tg*^{rol} (83.2 ± 2.1%, n = 3) mice, similar as observed in wt. In contrast to the small reduction by ω-CgTx in wt, there was a large decrease in PF-EPSC amplitude in *tg* (56.9 ± 4.3%, n = 4). A considerable reduction in PF-EPSCs, although to a lesser extent, was also observed in *tg*^{rol} (38.6 ± 4.7%, n = 3). The remaining component after application of both toxins was larger in *tg* (18.5 ± 5.0 %, n = 3) and *tg*^{rol} (22.9 ± 3.3 %, n = 3) than that of wt.

The sum of the ω-Aga-IVA-sensitive and ω-CgTx-sensitive EPSC fractions and the

EPSC fraction insensitive to both is larger than unity, showing an apparent overlap in the effect of ω-Aga-IVA and ω-CgTx on the synaptic currents. This overlap can be explained by a non-linear relation between the Ca^{2+} influx and EPSCs. In my estimation using a third power function from the data of PF-PC EPSCs, the sum of the estimated Ca^{2+} channel subtype fractions was close to unity in wt, but, the sums were over unity in mutant mice (Table 2). The estimated P/Q-type fraction was decreased from 55 % of wt to 45 % in *tg* and *tg*^{rol}, whereas the N-type fraction and the assumed R-type fraction increased in the mutants. The increase in the N-type fraction was more prominent in *tg* than in *tg*^{rol}, which may contribute to the difference in severity of ataxic phenotype between *tg* and *tg*^{rol}.

EPSCs at climbing fiber-Purkinje cell synapses in mutant mice

CF-mediated EPSCs (CF-EPSCs) were examined in parasagittal cerebellar slices from wt, *tg*, and *tg*^{rol} mice at P14-20, and from wt and *tg* at P28-35. Climbing fibers were stimulated locally in the granule cell layer, and CF-EPSCs of Purkinje cells were recorded in the whole-cell configuration. The holding potential was adjusted in every experimental condition to set the driving force to a constant value (20mV) for inward currents. CF-EPSCs could be clearly distinguished from PF-EPSCs by the following two criteria: (1) CF-EPSCs appeared with a discrete step when the stimulus intensity was increased gradually, (2) CF-EPSCs showed paired-pulse depression (PPD), in contrast to PF-PC EPSCs which exhibited PPF (Konnerth et al., 1990). In a majority of wt, *tg*, and *tg*^{rol} Purkinje cells, a large EPSC was elicited in all-or-none fashion without contamination of parallel fiber responses, as the stimulus intensity was gradually

increased (pulse width 100 μs, strength 0-100 V). In the three types of mice, the I-V relationship for the peak current amplitude was linear (data not shown). Whereas the peak amplitude of CF-EPSCs was unaltered in *tg*, that of tg^{rol} was significantly increased (Fig. 8). The results of unaltered or enhanced CF-EPSCs were surprising, because we expected reduced CF-EPSCs in ataxic mutant mice, as was the case for PF-EPSCs.

Properties of CF-EPSCs

To examine whether the kinetics of CF-EPSCs were altered in the mutant mice, we measured the 10-90% rise time and the decay time constant of CF-EPSCs in wt and mutant mice (Table 3). Whereas the 10-90% rise time was not significantly different among wt, *tg*, and tg^{rol} mice, the decay time constant of tg^{rol} was considerably greater than that of wt and *tg*. Thus, the tg^{rol} mutation of the P/Q-type Ca^{2+} channel results in not only an increased CF-PC EPSC amplitude but also alteration of CF-PC EPSC kinetics.

The slower decay time constant in tg^{rol} suggests a possibility that CF-EPSCs may be partly mediated by the NMDA receptor channels, which show slower activation and slower current decay than AMPA receptor channels. But CF-EPSCs were completely insensitive to APV (100 μM) in wt, *tg*, and tg^{rol}, whereas they were blocked by CNQX (10 μM) (Fig. 9). This result indicates that CF-EPSCs are mediated exclusively by non-NMDA receptors not only in wt and *tg* but also in tg^{rol}, consistent with previous reports of rat (Konnerth et al., 1990) and mouse (Aiba et al., 1994; Kano et al., 1995).

In contrast to PPF of PF-EPSCs, PPD is a characteristic feature of the CF-PC synapse, which results from decreased transmitter release from presynaptic terminals in response

to the second stimulus of a pair (Konnerth et al., 1990). In wt and tg^{rol}, CF-EPSCs exhibited considerable paired pulse depression at 50 ms interpulse intervals, but PPD of *tg* CF-EPSCs was significantly smaller than that of the wt or tg^{rol} CF-EPSCs (Fig. 10, Table 3). The *tg* mice develop ataxia about 3 weeks of age. To examine the relationship between CF-EPSCs and ataxia, we characterized the properties of CF-EPSCs of ataxic *tg* mice (P28-32). PPD was further reduced in adult ataxic *tg* mice compared to non-ataxic young *tg* mice, indicating that the reduced PPD was not directly related to ataxia. The amplitude, decay time constant, and rise time showed no difference (Table 3).

Firing pattern evoked by CF stimulation

In a native condition, Purkinje cells generate complex spikes in response to CF activation (Llinás and Walton, 1998). To see the effect of the Ca^{2+} channel mutations on firing pattern of Purkinje cells, complex spikes were recorded in a current-clamp mode (Fig. 11). Complex spikes can be generated in *tg* and tg^{rol}, and no obvious changes were observed.

Ca^{2+} channel subtypes in CF-PC synapses

Previous studies showed that both P/Q-type and N-type channels are present at CF terminals and play a critical role in neurotransmitter release, and that the P/Q-type channel contributes more (70-90 %) to the CF-PC synaptic transmission than the N-type channel (Regehr and Mintz, 1994; Doroshenko et al., 1997). We measured changes in CF-EPSCs to application of ω-Aga-IVA and ω-CgTx. Similar to earlier findings in rat cerebellum, application of 0.2 μM ω-Aga-IVA to the slices of wt partially blocked CF-

EPSCs (Fig. 12A, Table 4). CF-EPSCs were reduced by 51.6 ± 9.9 % (n = 4) of the baseline. On the other hand, application of 3 μM ω-CgTx reduced CF-EPSC by 13.4 ± 4.4% (n = 5) (Fig. 13A). Coapplication of 0.2 μM ω-Aga-IVA and 3 μM ω-CgTx eliminated the bulk of the synaptic current, leaving a small component (10.6 ± 3.4 %). Because the remaining component was not influenced by nifedipine (5 μM), it is likely to be an R-type channel-dependent component (Fig. 14). These results demonstrate that among the P/Q-, N-, and presumed R-type Ca^{2+} channels, the P/Q-type Ca^{2+} channel playing a predominant role for the CF-PC synaptic transmission.

When the same set of experiments was performed on *tg* and *tg*^{rol} slices, clear alterations in toxin sensitivity were observed. In contrast to the large decrease in CF-EPSCs by ω-Aga-IVA in wt, there was only a small reduction in CF-EPSC amplitude in *tg* (12.7 ± 6.4 %, n=3) and *tg*^{rol} (17.4 ± 9.6 %, n=3) (Fig.12, Table 4). In contrast, application of ω-CgTx caused a large decrease in CF-EPSC amplitude in *tg* (49.1 ± 1.5%, n = 3) and *tg*^{rol} (41.6 ± 12.2%, n=3) (Fig. 13). Subsequent coapplication of 0.2 μM ω-Aga-IVA and 3 μM ω-CgTx further reduced CF EPSCs, but the remaining component was much larger in *tg* (23.5 ± 6.5%) than wt (10.6 ± 3.4%). This component was not influenced by nifedipine (5 μM). These data show that, as we predicted, neurotransmitter release is less dependent on the P/Q-type channel in mutant mice.

The relative contribution of Ca^{2+} channel subtypes was estimated using the power function, as for the PF-EPSCs (Table 4). The presumed R-type fraction is unexpectedly large, and the sum of estimated fraction is far below the unity. These unsatisfactory estimates may due to deviation from the power relation caused by saturation of Ca^{2+} binding sites. When the saturation effect is taken into account, the relationship between

Ca^{2+} influx and EPSC can be described by the Hill's equation (Table 5). The estimates of fractional contribution are more consistent with earlier reports (Momiyama and Koga, 2001). In either model, the P/Q-type fraction is not so predominant as in PF-PC synapses. The presumed R-type plays a major role in wt, and its fraction, together with the N-type fraction, is also increased in mutants.

Miniature CF-EPSCs

The CF-EPSC decay time constant of tg^{rol} was larger than that of wt and *tg*. There are two kinds of hypothesis to explain the prolonged EPSC decay. Whereas CF stimulation usually generates synchronous neurotransmitter release at each synapse in wt mice, neurotransmitter release may be asynchronous in tg^{rol}, resulting in a prolonged decay time constant. The other possibility is that functional properties of the postsynaptic AMPA receptors are altered to cause a slower EPSC decay. Except during early development, Purkinje cells are innervated by both parallel and climbing fibers, which makes it difficult to measure CF miniature currents in isolation. We circumvented this problem by evoking CF-EPSCs in the presence of Sr^{2+} (Silver et al., 1998). Sr^{2+} can substitute Ca^{2+} in triggering neurotransmitter release, but it causes desynchronized release (Abdul-Ghani et al., 1996). Miniature EPSCs observed in a time window of 200 - 300 ms after stimulation were collected and analyzed. The decay time constant of tg^{rol} miniature CF-EPSCs was clearly larger than those of wt and *tg* (Fig. 15). The result is consistent with the prolonged decay time of macroscopic CF-EPSCs, and suggests functional alteration of postsynaptic AMPA receptors in tg^{rol}.

Enhanced AMPA sensitivity in tg^{rol} Purkinje cells

Because the prolonged decay time constant of whole-cell and miniature CF-EPSCs in tg^{rol} suggests a postsynaptic origin, whole-cell currents were examined in acutely dissociated Purkinje cells from wt, *tg*, and tg^{rol} mice in response to a glutamate receptor agonist. Cyclothiazide (100 μM) was always included in the external solution to reduce desensitization (Partin et al., 1993). Application of AMPA (1 - 300 μM) to Purkinje cells at a holding potential of -50 mV evoked rapidly activating inward currents at all cells tested. Measurements were made at the peak of the responses. Concentration-response relationships for AMPA-evoked currents were not significantly different between wt (EC_{50} 53.1 ± 5.3 μM, Hill coefficient 1.1, maximum current dencity (I_{max}) 252.2 ± 26.5 pA/pF, n = 12) and *tg* (EC_{50} 48.7 ± 6.4 μM, Hill coefficient 1.0, I_{max} 217.2 ± 12.3 pA/pF, n = 9). In contrast, the relationship of tg^{rol} (EC_{50}; 15.2 ± 2.0 μM, n = 8) was shifted in the direction of lower concentrations compared with those of wt and *tg*, but there were no significant differences in Hill coefficient (1.17 ± 0.03) or I_{max} value (247.9 ± 51.7 pA/pF) obtained (Fig. 16). These results suggest that the increase in the CF-PC response in tg^{rol} mice is at least partly due to hyper-sensitivity of the AMPA receptors to glutamate.

Ca^{2+} dependence of PF-EPSC and CF-EPSC

The effects of the Ca^{2+} channel mutations are surprisingly different on PF-EPSC and CF-EPSC. Whereas the PF-EPSC amplitude is depressed in mutants, the CF-EPSC amplitude is unchanged or even increased. Although different compensatory mechanisms for the mutations are partly responsible for the distinct responses, I assume

that the PF-PC and CF-PC synapses are functionally very different. One of the significant differences is the Ca^{2+} dependence of EPSC. As shown by the effects on EPSC of toxin application, the PF-EPSC amplitude can be simulated by a power relation, whereas the saturation effect should be considered for CF-EPSC. To test the validity of the estimation of Ca^{2+} channel fractions using the power relation or the Hill's equation, the effect of lowering the external Ca^{2+} concentration on EPSC amplitude was studied (Fig. 17). The PF-EPSC amplitude was very sensitive to lowering the external Ca^{2+} concentration. When the normalized PF-EPSC amplitude was fit by a power relation, the m value was 1.7, significantly lower than the commonly used value (m = 3 ~ 4). The normalized CF-EPSC was well fit by the Hill's equation, with the relative half-saturation concentration $d = 0.29$.

DISCUSSION

Cerebellar ataxia caused by P/Q-type Ca^{2+} channel mutations

Cerebellar ataxia is a common neurological abnormality among the Ca^{2+} channel α_{1A} subunit mutant mice, which include *tg* and tg^{rol}. Severity of cerebellar ataxia, however, differs significantly between *tg* and tg^{rol} mice. Homozygous *tg* mice do not show ataxic symptoms until 3~4 weeks of age, whereas homozygous tg^{rol} mice start showing ataxic behaviors around P10. Also ataxic symptoms are severer in tg^{rol} than *tg*. Although loss or degeneration of cerebellar neurons was reported in leaner mutant mice (tg^{la}), which exhibits even severer ataxia than tg^{rol} (Herrup and Wilczynski, 1982), there is no conclusive evidence to indicate that ataxia results from neuronal death or degeneration in *tg* or tg^{rol}. Previous results suggest that the degree of deviation of the P/Q-type Ca^{2+} channel function in Purkinje cells is somewhat correlated with the severity of cerebellar symptoms in mutant strains *tg*, tg^{la} (Wakamori et al., 1998) and tg^{rol} (Mori et al., 2000). In tg^{la} Purkinje cells, P/Q-type Ca^{2+} channel current is reduced by ~60%, whereas P/Q-type Ca^{2+} current amplitude is reduced by ~40% in *tg* and tg^{rol} Purkinje cells. In tg^{rol}, however, the voltage dependence of activation of the P/Q-type channel shows a depolarizing shift because of the mutation in the voltage sensing S4 transmembrane segment. This change in voltage dependence would further reduce the Ca^{2+} influx in native conditions in the brain.

Reduced PF-PC EPSCs and onset ataxia

PF stimulation was consistently less effective to elicit PF-EPSCs in *tg* and ataxic tg^{rol} Purkinje cells than wt Purkinje cells in the stimulation intensity range from 3 to 15 volts.

Moreover, whereas P14-20 *tg* mice, which do not have obvious ataxia showed about 30% reduction in the amplitude, clearly ataxic *tg* mice at P28-35 exhibited a more dramatic reduction (~70%) in PF-EPSC amplitude, indicating a close relationship between impaired PF-PC synaptic transmission and cerebellar ataxia. The present results are consistent with the previous reports that ataxia is associated with dysfunction of the PF-PC system. In stargazer mutant mice, which have a disrupted stargazin/putative neuronal Ca^{2+} channel γ subunit (Letts et al., 1998), EPSCs at the mossy fiber (MF)-granule cell (GC) synapses are devoid of the AMPA receptor-mediated fast component. Consequently, the amplitudes of PF-EPSCs and CF-EPSCs were ~60% of control (Hashimoto et al., 1999). The waggler mice, an ataxic mutant strain with a disrupted putative neuronal Ca^{2+} channel γ subunit have reduced transmission at PF-PC synapse, and multiple synapses of cerebellar granule cells arrested at an immature stage during development (Chen et al., 1999). In GluR2δ-knock out mice, the number of PF-PC synapses is reduced by half, mainly because of impaired synaptic contact of Purkinje cell spines, and PF stimulation is consistently less effective to elicit PF-EPSCs (Kurihara et al., 1997). The previous studies, however, have provided no clue for the temporal relationship between the PF-PC synaptic dysfunction and the onset of ataxia. The present results of the impaired PF response show evidence that the dysfunction of the PF-PC synaptic transmission underlies cerebellar ataxia.

Purkinje cell firing of simple spikes normally ranges from 50 to 100 Hz depending on the strength of PF inputs (Ebner, 1998). The frequency of simple spikes is considered to encode centrally generated behaviors. In fact, voluntary eye or limb movements are associated with a marked change in simple spike frequency. Moreover, the PF-PC

synapse can undergo long-term modifications in synaptic strength, and such plasticity has been suggested to underlie motor learning (Ito, 1986). The dysfunction of PF-PC synaptic transmission in *tg* and *tg^{rol}* thus not only blocks the transmission of centrally encoded behaviors to generate voluntary movements but also impairs fine tunings of neural circuits.

Properties of PF-PC synapse in mutant mice

Although it was reported that the Ca^{2+} channels which contribute synaptic transmission at PF-PC are mostly P/Q-type (~99%) (Mintz et al., 1995), the contribution of the P/Q type to PF-EPSCs was smaller in my present study. Application of ω-Aga-IVA abolished 80-90% of PF-PC synaptic transmission in wt, *tg*, and *tg^{rol}*. These results suggest that the contribution of the P/Q-type channels remains predominant in *tg* and *tg^{rol}*. On the other hand, the ω-CgTx sensitive component was relatively increased in *tg*. When the fractional contribution of Ca^{2+} channel subtypes to PF-EPSC was estimated using the power relationship, the fractional contribution of the P/Q-type is about a half, and interestingly the presumed R-type is the second major component in wt. In the mutant synapses, the contribution of the N-type is increased, but it remained a minor component. The R-type is likely the predominant Ca^{2+} channel subtype in PF terminals in mutant mice. In my estimation using a third power function from the data of PF-PC EPSCs, the sum of the estimated Ca^{2+} channel subtype fractions was close to unity in wt, but, the sums were over unity in mutant mice (Table 2). This result suggest that the presynaptic terminals in mutant mice may be less efficient in triggering neurotransmitter release than wt.

In this study, PPF at the PF-PC synapse was increased in tg^{rol}. PPF is a presynaptic phenomenon believed to strongly depend on residual $[Ca^{2+}]_i$ in the presynaptic terminal (Zucker et al., 1989). In tg^{rol}, a compromised amount of Ca^{2+} enters into presynaptic terminal after the first pulse, giving a very small amount of neurotransmitter release, according to the power relation. But the second pulse generates Ca^{2+} influx, which can cause transmitter release more effectively due to the residual Ca^{2+}. Thus the increased PPF is likely to be a consequence of severely reduced Ca^{2+} influx in tg^{rol}. It is also possible, however, that mutant mice have altered Ca^{2+} buffering capacity or release mechanism as secondary phenomena of the mutations. In fact, indirect effects of the mutations were demonstrated to occur in mutant mice. The previous ultrastructural analyses showed that the number of PF nerve terminals having multiple contacts with dendritic spines of Purkinje cells is increased in *tg* and tg^{rol} (Rhyu et al., 1999a; Rhyu et al., 1999b). Such structural reorganization may also contribute to partially compensating for reduction of neurotransmitter release per synaptic contact of *tg* and tg^{rol} Purkinje cells.

Paradoxically enhanced CF-EPSCs in tg^{rol}

The previous studies demonstrated that the *tg* and tg^{rol} mutations reduce the P/Q-type Ca^{2+} channel currents directly (Wakamori et al., 1998; Mori et al., 2000). Because the P/Q-type is a major Ca^{2+} channel in CF nerve terminals, I expected that CF-EPSCs would be very much reduced. In this study, however, at the CF-PC synapse, the mean of amplitude and the decay time constant of CF-EPSCs were unchanged in *tg*, and surprisingly, the CF-EPSC amplitude was increased significantly and the decay time

constant was prolonged in tg^{rol} mice.

To uncover the mechanism of enhanced CF-PC in tg^{rol}, I measured the decay time constant of miniature CF-EPSCs as well as AMPA sensitivity of acutely dissociated Purkinje cells. The decay time constant of tg^{rol} miniature CF-EPSCs was larger than those of wt and *tg*. The AMPA receptors of tg^{rol} showed a higher sensitivity to AMPA. Those results suggest that the enhanced CF-EPSCs with slower decay are caused by a postsynaptic mechanism. The CF-PC responses are glutamatergic and are known to be mediated by the AMPA receptors (Llano et al., 1991). Because CF-EPSCs were blocked by CNQX, but completely insensitive to APV not only in wt and *tg*, but also in tg^{rol}, the alteration of CF-EPSCs in tg^{rol} is not attributable to aberrant expression of NMDA receptor channels. The AMPA receptors have four kinds of subunits (GluR1-4), and each subunit has two alternative splicing forms, flip and flop. The AMPA receptor channels are thought to be assembled from each of the subunits alone or from their combinations. Such different compositions confer functionally different properties on the AMPA receptor channels (Burnashev et al., 1992; Geiger et al., 1995). In Purkinje neurons, GluR2 and GluR3 are the predominant subunits. Preliminary *in situ* hybridization studies failed to reveal significant changes in expression of GluR1-4 in mutant Purkinje cells. Because it is reported that the flip forms have a higher agonist affinity and a slower decay and that the flip forms are replaced by the flop forms developmentally, it is conceivable that the flip forms of GluR2 and GluR3 are predominantly expressed in tg^{rol} CF-PC synapses, resulting in the enhanced AMPA sensitivity and the prolonged decay time constant of CF-EPSCs. Thus, the results suggest that the tg^{rol} mutation has altered the subunit composition of the postsynapitc

AMPA receptors, presumably through the reduction in Ca^{2+} influx to dendrites of Purkinje cells causing delay of, or deviation from, the normal development. It is interesting to note that the kinetics of PF-EPSC remained unchanged in *tg* and *tg*^{rol}, indicating that the organization and properties of the PF-PC and CF-PC synapses are regulated separately.

Responses of the AMPA receptors are greatly influenced by glutamate transporters, which are expressed in Purkinje cells and Bergmann glial cells in the cerebellum (Bergles et al., 1997; Auger and Attwell, 2000). The possibility that alteration of properties of glutamate transporters can cause the increased AMPA sensitivity and the prolonged CF-EPSC decay cannot be excluded.

Properties of CF-PC synapses in mutant mice

Synaptic transmission at CF-PC synapses in mutant mice remained by and large intact. Although the alteration of the postsynaptic AMPA receptors contributes to maintaining normal CF-PC synaptic transmission in the case of *tg*^{rol}, there should be other compensatory mechanisms for *tg* mice.

To examine the possibility that other Ca^{2+} channel subtypes are increased in mutant CF nerve terminals, I estimated the contribution of the P/Q- and N-types to neurotransmitter release using the Hill's equation. The fractional contributions to CF-EPSC of the P/Q-, N-, and presumed R-types are about 45%, 20%, and 35%, respectively. In *tg* and *tg*^{rol}, the P/Q-type fraction decreased to ~20%, and the N- and presumed R-type components increased to ~40% each. Because direct measurement of presynaptic Ca^{2+} concentration was not made, it is difficult to estimate absolute changes

of the N- and presumed R-type components. But the elevated ratio of N-type to R-type strongly suggests that the N-type channel component is actually elevated in mutant mice, and this increase certainly contributes to maintain the CF-PC synaptic transmission. Although the role of the presumed R-type in compensating the mutated P/Q-type channel is not so evident, the CF-PC synaptic transmission is more dependent on the N-type and presumed R-type channels in mutant mice. A similar change has been reported in hippocampal synapses of *tg* mice (Qian and Noebels, 2000).

Ca^{2+} channels involved in neurotransmitter release switch developmentally from the N-type to the P/Q-type at various mammalian fast synapses (Iwasaki et al., 2000). The contribution of the N-type is lost during postnatal development in cerebellar and thalamic inhibitory synapses, rat auditory brainstem excitatory synapses (Iwasaki and Takahashi, 1998), and neuromuscular junctions (Rosato Siri and Uchitel, 1999). Although no data of developmental switching of Ca^{2+} channel types are available for the cerebellar CF-PC synapses, the increased N-type component in *tg* and tg^{rol} may be regarded as delayed neuronal maturation, if the CF-PC synapses physiologically undergo developmental switching from the N-type to the P/Q-type.

The morphological observations of tg^{rol} Purkinje cells support the notion of the deranged developmental switching. Ultrastructural analyses demonstrated numerous spine formations in the proximal dendrites in tg^{rol}. Similar morphological changes were reported to occur in early developmental stages (Altman and Bayer, 1997). Climbing fibers form synapses on the protuberances of Purkinje cell soma and stem dendrites. In addition, hyperspiny transformation of the proximal dendrites is also observed in the cerebellum where neuronal activity is blocked by tetrodotoxin (Bravin et al., 1999).

Since Ca^{2+} functions as an indicator of neuronal activity, impaired Ca^{2+} influx into tg^{rol} Purkinje cell dendrites may cause delayed developmental switching and formation of ectopic dendritic spines.

In this study, the magnitude of PPD of the *tg* CF-PC synapse was smaller than those of wt and tg^{rol}. Short-term depression is a widespread form of use-dependent plasticity found in the peripheral and central nervous systems of invertebrates and vertebrates (Dobrunz and Stevens, 1997). Generally PPD is explained by several different mechanisms; presynaptic depletion of release-competent vesicles (Dittmann and Regehr, 1998), other presynaptic factors transiently depressing vesicle release probability or the level of presynaptic Ca^{2+} entry (Hsu et al., 1996). Since PPD is reduced in *tg* without affecting the CF-EPSC amplitude, this finding may suggest that Ca^{2+} exerts a different depressing activity, depending on the Ca^{2+} channel subtypes through which Ca^{2+} entered into cells.

PF-PC synapses and CF-PC synapses

Cerebellar Purkinje neurons have two major sources of excitatory inputs, parallel fibers and climbing fibers. In this study, the two fiber systems showed a marked difference in the effects caused by the mutations of the P/Q-type Ca^{2+} channel. Whereas the PF-Purkinje synapses showed severe impairments that correlated to the ataxic symptom, the evoked CF-Purkinje responses remained intact or even enhanced. As shown in paired-pulse responses, the PF-Purkinje cell synapses have a rather low probability of neurotransmitter release in the normal range of Ca^{2+} concentration. The Ca^{2+} concentration is far below the saturating level, and the relationship between the Ca^{2+}

concentration and the neurotransmitter release can be reasonably described by the power relation. Thus, a small reduction in Ca^{2+} influx causes a great reduction in transmitter release. These conditions make the PF-Purkinje synapses more vulnerable to alterations of the presynaptic Ca^{2+} channels. In contrast, the CF-Purkinje cell synapses have the large number of release sites, the large quantal size and high release probability, all of which would ensure that transmission at the CF synaptic connection is highly reliable at low frequencies. Strong PPD seen at these synapses, along with little increase in synaptic strength with elevated external Ca^{2+}, indicate that release probability is near maximal (Dittman and Regehr, 1998; Silver et al., 1998). The significant difference in dependence on the external Ca^{2+} concentration of the PF-EPSC and CF-EPSC amplitudes were clearly validated in this study (Fig. 17).

Changing the external Ca^{2+} concentration from 0.5 to 1mM greatly enhances synaptic strength, further increases in the external Ca^{2+} concentration have little effect on the CF synaptic strength, suggesting that that the CF-PC synapse operates at high baseline release probability (Dittman and Regehr, 1998). This behavior is a hallmark of the CF synapse that operates near saturation and is in sharp contrast to nonsatulated synapse, such as the PF-PC synapse, where doubling external Ca^{2+} can enhance synaptic strength 10-fold (Zucker, 1989). However, previous studies did not compare the dependence on the external Ca^{2+} of CF- and PF-EPSC amplitudes explicitly. In this study, I studied the CF-PC and PF-PC synapses, and obtained the results that the PF-EPSC amplitude is reduced significantly by slightly lowering the external Ca^{2+} concentration, whereas the CF-EPSC amplitude was little affected. Thus the different responses to the mutations between the PF-PC and CF-PC synapses are at least partly explained by the difference

in the strength of synaptic connections, through a different dependence on external Ca^{2+} concentration. To support this notion, the mutant mice have practically intact neuromuscular transmission, which is dependent on the P/Q-type calcium channel and has a high safety margin (Plomp et al., 2000).

Altered P/Q-type channel function and neurological phenotypes

Because the P/Q type is the predominant Ca^{2+} channel type in the central nervous system, it is rather surprising that the neurological dysfunctions are mostly confined to the cerebellum in the P/Q-type Ca^{2+} channel mutant mice. Besides cerebellar ataxia, however, some of the mutant mice show additional neurological phenotypes. The *tg*, tg^{la}, and rkr mice display absence epilepsy (Burgess and Noebles, 1999; Zwingman et al., 2000), whereas tg^{rol} mice do not (Oda, 1981). It is interesting how the diversity of neurological phenotypes is generated. I propose that different neuronal populations have different levels of tolerance for the functional deviation of the P/Q type channel. One important factor is the compensatory mechanism. When the P/Q type channel is defective, other types of Ca^{2+} channels, such as N- and R-types, compensate the mutational effect. But it appears that different neuronal populations show different flexibility for compensatory mechanism. To support this notion, the previous report demonstrated that hippocampal inhibitory interneurons have preference for the P/Q- or N-type Ca^{2+} channel subtypes (Poncer et al., 1997). In hippocampus, Inhibitory neurons in stratum lucidum and stratum oriens use only the P/Q-type channel, as indicated by the fact that inhibitory postsynaptic potentials onto pyramidal neurons are sensitive only to P/Q-type but not N-type channel blockers, whereas other interneurons are purely

dependent on the N-type channel. Thus, P/Q-type channel mutations would disproportionately affect the function of this subset of neurons and similar populations throughout the nervous system, consequently impair synaptic transmission and thereby disrupt the balance of neuronal excitation and inhibition. If neurological symptoms are caused by such deviations from a finely tuned balance between excitatory and inhibitory networks, knockout mice in which a functional molecule is completely eliminated may not serve as appropriate models for neurological disorders. In the null mutant mice lacking the expression of the α_{1A} subunit, a complete loss of P/Q-type Ca^{2+} channel function induces an ataxia that progressively worsened up to the point of premature death (Jun et al., 1999).

Mutations of the Ca^{2+} channel α_{1A} subunit are associated with some human inherited neurological diseases. Missense mutations, nonsense mutations, and CAG expansion have been shown to underlie neurological disorders such as familial hemiplegic migraine, episodic ataxia type-2 (Ophoff et al., 1996), and autosomal dominant spinocerebellar ataxia (SCA6) (Zhuchenko et al., 1997). Interestingly all the human diseases caused by P/Q-type calcium channel mutations are dominantly inherited, whereas the mouse disorders are autosomal recessive. This does not imply that the mechanism of pathogenesis is different between mice and human. In fact, we can detect subtle abnormalities in synaptic transmission in the hippocampus of heterozygous *tg* mice (Matsushita et al., Personal observation). The observation indicates that even slight impairment of Ca^{2+} channel function can lead to dysfunction of the brain, and underscores the necessity of tight and fine regulation of Ca^{2+} channels to maintain normal brain functions. Relatively mild symptoms can be recognized in human. But in

case of mice, we can detect only prominent manifestations, and subtle symptoms may be easily overlooked. This fact has to be taken into account when we try to extrapolate the results of model animals to understanding human diseases.

REFERENCES

Abdul-Ghani MA, Valiante TA, Pennefather PS (1996) Sr^{2+} and quantal events at excitatory synapses between mouse hippocampal neurons in culture. J Physiol 5:113-125.

Aiba A, Kano M, Chen C, Stanton ME, Fox GD, Herrup K, Zwingman TA, Tonegawa S (1994) Deficient cerebellar long-term depression and impaired motor learning in mGluR1 mutant mice. Cell 79: 377-388.

Altman J and Bayer S (1997) Development of the cerebellar system. Boca Raton, FL CRC press: pp446-451

Altman J, McCrady B (1972) The influence of nutrition on neural and behavioral development. IV. Effects of infantile undernutrition on the growth of the cerebellum. Dev Psychobiol 5: 111-122.

Artalejo CR, Adams ME, Fox AP (1994) Three types of Ca^{2+} channel trigger secretion with different efficacies in chromaffin cells. Nature 367: 72-76.

Auger C, Attwell D (2000) Fast removal of synaptic glutamate by postsynaptic transporters. Neuron 28: 547-558.

Bergles DE, Dzubay JA, Jahr CE (1997) Glutamate transporter currents in bergmann glial cells follow the time course of extrasynaptic glutamate. Proc Natl Acad Sci USA 94: 14821-14825.

Bourinet E, Soong TW, Sutton K, Slaymaker S, Mathews E, Monteil A, Zamponi GW, Nargeot J, Snutch TP (1999) Splicing of alpha α_{1A} subunit gene generates phenotypic variants of P- and Q-type calcium channels. Nat Neurosci 2: 407-415.

Burgess DL, Noebels JL (1999) Single gene defects in mice: the role of voltage-dependent calcium channels in absence models. Epilepsy Res 36: 111-122.

Bravin M, Morando L, Vercelli A, Rossi F, Strata P (1999) Control of spine formation by electrical activity in the adult rat cerebellum. Proc Natl Acad Sci USA 96: 1704-

1709.

Burnashev N, Khodorova A, Jonas P, Helm PJ, Wisden W, Monyer H, Seeburg PH, Sakmann B (1992) Calcium-permeable AMPA-kainate receptors in fusiform cerebellar glial cells. Science 256: 1566-1570.

Catterall WA (2000) Structure and regulation of voltage-gated Ca^{2+} channels. Annu Rev Cell Dev Biol 16: 521-555.

Chen L, Bao S, Qiao X, Thompson RF (1999) Impaired cerebellar synapse maturation in waggler, a mutant mouse with a disrupted neuronal calcium channel γ subunit. Proc Natl Acad Sci USA 96: 12132-12137.

Dittman JS, Regehr WG (1998) Calcium dependence and recovery kinetics of presynaptic depression at the climbing fiber to Purkinje cell synapse. J Neurosci 18: 6147-6162.

Dobrunz LE, Stevens CF (1997) Heterogeneity of release probability, facilitation, and depletion at central synapses. Neuron 18: 995-1008.

Dodge FA Jr, Rahamimoff R (1967) Co-operative action a calcium ions in transmitter release at the neuromuscular junction. J Physiol 193: 419-432

Doroshenko PA, Woppmann A, Miljanich G, Augustine GJ (1997) Pharmacologically distinct presynaptic calcium channels in cerebellar excitatory and inhibitory synapses. Neuropharmacology 36: 865-872

Ebner TJ (1998) A role for the cerebellum in the control of limb movement velocity. Curr Opin Neurobiol 8: 762-769.

Edwards FA, Konnerth A, Sakmann B, Takahashi T (1989) A thin slice preparation for patch clamp recordings from neurones of the mammalian central nervous system. Pflügers Arch 414: 600-612.

Fletcher CF, Lutz CM, O'Sullivan TN, Shaughnessy JD Jr, Hawkes R, Frankel WN, Copeland NG, Jenkins NA (1996) Absence epilepsy in tottering mutant mice is

associated with calcium channel defects. Cell 87: 607-617.

Geiger JR, Melcher T, Koh DS, Sakmann B, Seeburg PH, Jonas P, Monyer H (1995) Relative abundance of subunit mRNAs determines gating and Ca^{2+} permeability of AMPA receptors in principal neurons and interneurons in rat CNS. Neuron 15: 193-204.

Ghosh A, Greenberg ME (1995) Calcium signaling in neurons: molecular mechanisms and cellular consequences. Science 268: 239-247.

Green MC, Sidman RL (1962) Tottering- a neuromuscular mutation in the mouse. J Hered 53: 233-237

Hashimoto K, Fukaya M, Qiao X, Sakimura K, Watanabe M, Kano M (1999) Impairment of AMPA receptor function in cerebellar granule cells of ataxic mutant mouse stargazer. J Neurosci 19: 6027-6036.

Herrup K, Wilczynski SL (1982) Cerebellar cell degeneration in the leaner mutant mouse. Neuroscience 7: 2185-2196.

Hirning LD, Fox AP, McCleskey EW, Olivera BM, Thayer SA, Miller RJ, Tsien RW (1988) Dominant role of N-type Ca^{2+} channels in evoked release of norepinephrine from sympathetic neurons. Science 239: 57-61.

Hsu SF, Augustine GJ, Jackson MB (1996) Adaptation of Ca^{2+}-triggered exocytosis in presynaptic terminals. Neuron 17: 501-512.

Ito M (1986) Long-term depression as a memory process in the cerebellum. Neurosci Res 3: 531-539.

Iwasaki S, Takahashi T (1998) Developmental changes in calcium channel types mediating synaptic transmission in rat auditory brainstem. J Physiol 509: 419-423.

Iwasaki S, Momiyama A, Uchitel OD, Takahashi T (2000) Developmental changes in calcium channel types mediating central synaptic transmission. J Neurosci 20: 59-65.

Jun K, Piedras-Renteria ES, Smith SM, Wheeler DB, Lee SB, Lee TG, Chin H, Adams

ME, Scheller RH, Tsien RW, Shin HS (1999) Ablation of P/Q-type Ca^{2+} channel currents, altered synaptic transmission, and progressive ataxia in mice lacking the α_{1A}-subunit. Proc Natl Acad Sci USA 96: 15245-15250.

Kano M, Hashimoto K, Chen C, Abeliovich A, Aiba A, Kurihara H, Watanabe M, Inoue Y, Tonegawa S (1995) Impaired synapse elimination during cerebellar development in PKC gamma mutant mice. Cell 83: 1223-1231.

Konnerth A, Llano I, Armstrong CM (1990) Synaptic currents in cerebellar Purkinje cells. Proc Natl Acad Sci USA 87: 2662-2665.

Kurihara H, Hashimoto K, Kano M, Takayama C, Sakimura K, Mishina M, Inoue Y, Watanabe M (1997) Impaired parallel fiber -> Purkinje cell synapse stabilization during cerebellar development of mutant mice lacking the glutamate receptor δ2 subunit. J Neurosci 17: 9613-9623.

Letts VA, Felix R, Biddlecome GH, Arikkath J, Mahaffey CL, Valenzuela A, Bartlett FS 2nd, Mori Y, Campbell KP, Frankel WN (1998) The mouse stargazer gene encodes a neuronal Ca^{2+}-channel gamma subunit. Nat Genet 19: 340-347.

Llano I, Marty A, Armstrong CM, Konnerth A (1991) Synaptic- and agonist-induced excitatory currents of Purkinje cells in rat cerebellar slices. J Physiol 434: 183-213.

Llinás R, Sugimori M, Lin JW, Cherksey B. (1989) Blocking and isolation of a calcium channel from neurons in mammals and cephalopods utilizing a toxin fraction (FTX) from funnel-web spider poison. Proc Natl Acad Sci USA 86: 1689-1693.

Llinás R, Walton D (1998) Cerebellum. In: The synaptic organization of the brain. 4th ed (Shepherd GM, ed), pp 255-287, New York: Oxford UP.

Mintz IM, Sabatini BL, Regehr WG (1995) Calcium control of transmitter release at a cerebellar synapse. Neuron 15: 675-688.

Mintz IM, Venema VJ, Swiderek KM, Lee TD, Bean BP, Adams ME (1992) P-type calcium channels blocked by the spider toxin ω-Aga-IVA. Nature 355: 827-829.

Momiyama T, Koga E (2001) Dopamine D_2-like receptors selectively block N-type Ca^{2+} channels to reduce GABA release onto rat striatal cholinergic interneurones. J Physiol 533: 479-492.

Mori Y, Friedrich T, Kim MS, Mikami A, Nakai J, Ruth P, Bosse E, Hofmann F, Flockerzi V, Furuichi T, Mikoshiba K, Imoto K, Tanabe T, Numa S (1991) Primary structure and functional expression from complementary DNA of a brain calcium channel. Nature 350: 398-402.

Mori Y, Wakamori M, Oda S, Fletcher CF, Sekiguchi N, Mori E, Copeland NG, Jenkins NA, Matsushita K, Matsuyama Z, Imoto K (2000) Reduced voltage sensitivity of activation of P/Q-type Ca^{2+} channels is associated with the ataxic mouse mutation rolling Nagoya (*tg^{rol}*). J Neurosci 20: 5654-5662.

Oda S (1973) The observation of rolling mouse Nagoya (rol), a new neurological mutant, and its maintenance. Jikken Dobutsu 22: 281-288.

Oda S (1981) A new allele of tottering locus, rolling mouse Nagoya on chromosome No.8 in the mouse. Jpn J Genetics 56: 295-299.

Ophoff RA, Terwindt GM, Vergouwe MN, van Eijk R, Oefner PJ, Hoffman SM, Lamerdin JE, Mohrenweiser HW, Bulman DE, Ferrari M, Haan J, Lindhout D, van Ommen GJ, Hofker MH, Ferrari MD, Frants RR (1996) Familial hemiplegic migraine and episodic ataxia type-2 are caused by mutations in the Ca^{2+} channel gene CACNL1A4. Cell 87: 543-552.

Partin KM, Patneau DK, Winters CA, Mayer ML, Buonanno A (1993) Selective modulation of desensitization at AMPA versus kainate receptors by cyclothiazide and concanavalin A. Neuron 11: 1069-1082.

Poncer JC, McKinney RA, Gahwiler BH, Thompson SM (1997) Either N- or P-type calcium channels mediate GABA release at distinct hippocampal inhibitory synapses. Neuron 18: 463-472.

Plomp JJ, Vergouwe MN, Van den Maagdenberg AM, Ferrari MD, Frants RR, Molenaar PC (2000) Abnormal transmitter release at neuromuscular junctions of mice carrying the tottering alpha$_{1A}$ Ca^{2+} channel mutation. Brain 123, 463-471.

Qian J, Noebels JL (2000) Presynaptic Ca^{2+} influx at a mouse central synapse with Ca^{2+} channel subunit mutations. J Neurosci 20: 163-170.

Regan LJ, Sah DW, Bean BP (1991) Ca^{2+} channels in rat central and peripheral neurons: high-threshold current resistant to dihydropyridine blockers and ω-conotoxin. Neuron 6: 269-280.

Regehr WG, Mintz IM (1994) Participation of multiple calcium channel types in transmission at single climbing fiber to Purkinje cell synapses. Neuron 12: 605-613.

Rhyu IJ, Abbott LC, Walker DB, Sotelo C (1999a) An ultrastructural study of granule cell/Purkinje cell synapses in tottering (*tg/tg*), leaner (tg^{la}/tg^{la}) and compound heterozygous tottering/leaner (tg/tg^{la}) mice. Neuroscience 90: 717-728.

Rhyu IJ, Oda S, Uhm CS, Kim H, Suh YS, Abbott LC (1999b) Morphologic investigation of rolling mouse Nagoya (tg^{rol}/tg^{rol}) cerebellar Purkinje cells: an ataxic mutant, revisited. Neurosci Lett 266: 49-52.

Rosato Siri MD, Uchitel OD (1999) Calcium channels coupled to neurotransmitter release at neonatal rat neuromuscular junctions. J Physiol 514: 533-540.

Sather WA, Tanabe T, Zhang JF, Mori Y, Adams ME, Tsien RW (1993) Distinctive biophysical and pharmacological properties of class A (BI) calcium channel alpha 1 subunits. Neuron 11: 291-303.

Sidman RL, Green MC, Appel SH (1965) Catalog of the neurological mutants of the mouse. Cambridge, MA: Harvard UP.

Silver RA, Momiyama A, Cull-Candy SG (1998) Locus of frequency-dependent depression identified with multiple-probability fluctuation analysis at rat climbing

fibre-Purkinje cell synapses. J Physiol 510: 881-902.

Stea A, Tomlinson WJ, Soong TW, Bourinet E, Dubel SJ, Vincent SR, Snutch TP (1994) Localization and functional properties of a rat brain alpha 1A calcium channel reflect similarities to neuronal Q- and P-type channels. Proc Natl Acad Sci USA 25: 10576-10580.

Stühmer W, Conti F, Suzuki H, Wang XD, Noda M, Yahagi N, Kubo H, Numa S (1989) Structural parts involved in activation and inactivation of the sodium channel. Nature 339: 597-603.

Takahashi T, Momiyama A (1993) Different types of calcium channels mediate central synaptic transmission. Nature 366: 156-158.

Tsien RW, Tsien RY (1990) Calcium channels, stores, and oscillations. Annu Rev Cell Biol 6: 715-760.

Turner TJ, Adams ME, Dunlap K (1992) Calcium channels coupled to glutamate release identified by ω-Aga- IVA. Science 258: 310-313.

Wakamori M, Hidaka H, Akaike N (1993) Hyperpolarizing muscarinic responses of freshly dissociated rat hippocampal CA1 neurones. J Physiol 463: 585-604.

Wakamori M, Yamazaki K, Matsunodaira H, Teramoto T, Tanaka I, Niidome T, Sawada K, Nishizawa Y, Sekiguchi N, Mori E, Mori Y, Imoto K (1998) Single tottering mutations responsible for the neuropathic phenotype of the P-type calcium channel. J Biol Chem 273: 34857-34867.

Zhang JF, Randall AD, Ellinor PT, Horne WA, Sather WA, Tanabe T, Schwarz TL, Tsien RW (1993) Distinctive pharmacology and kinetics of cloned neuronal Ca^{2+} channels and their possible counterparts in mammalian CNS neurons. Neuropharmacology 32: 1075-1088.

Zhuchenko O, Bailey J, Bonnen P, Ashizawa T, Stockton DW, Amos C, Dobyns WB, Subramony SH, Zoghbi HY, Lee CC (1997) Autosomal dominant cerebellar ataxia (SCA6) associated with small polyglutamine expansions in the alpha 1A-voltage-

dependent calcium channel. Nat Genet 15: 62-69.

Zucker RS (1989) Short-term synaptic plasticity. Annu Rev Neurosci 12: 13-31.

Zwingman TA, Neumann PE, Noebels JL, Herrup K (2001) Rocker is a new variant of the voltage-dependent calcium channel gene Cacna1a. J Neurosci 21: 1169-1178.

Acknowledgments

I would like to express my sincere appreciation to Dr. Keiji Imoto, Dr. Yasuo Mori, Dr. Minoru Wakamori, and Dr. Junich Nakai, for their generous support and valuable guidance through this study. I am also sincerely grateful to Dr. Toshihiko Momiyama and Dr. Akiko Momiyama for their helpful discussion and advice. I would like to Ms. Naomi Sekiguchi for her excellent technical assistance. I wish to thank all the members of Division of Humoral Information for the support and kindness.

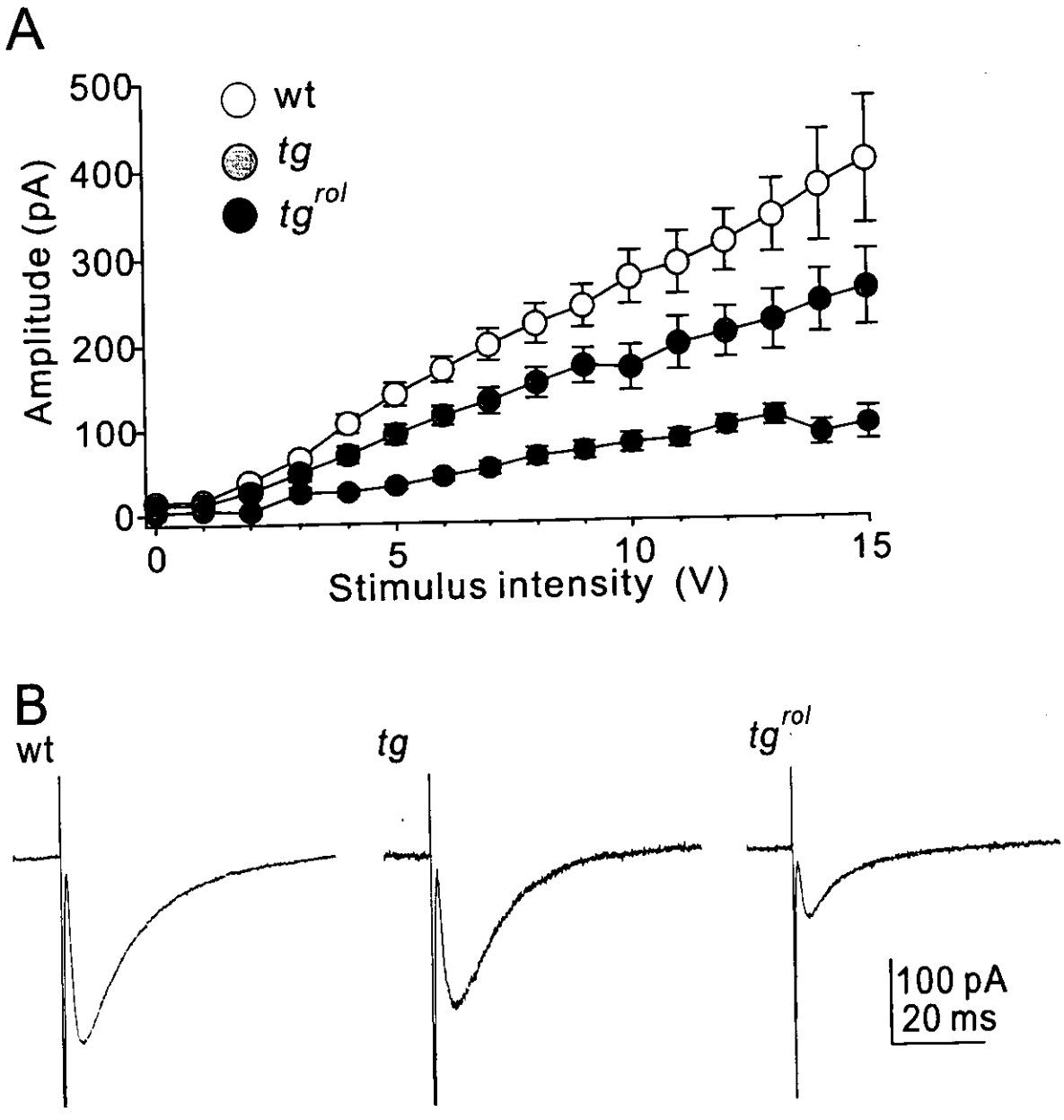
A
500
400
300
200
100
0
Amplitude (pA)
wt
tg
tg rol
0
5
10
15
Stimulus intensity (V)
B
wt
tg
tg rol
100 pA
20 ms

Fig.1.

Fig. 1. PF-PC synaptic transmission in mutant mice

A. PF-EPSC peak amplitudes were plotted against the intensity of stimulation for wt and mutant mice at P14-20. Averaged peak amplitudes were shown for wt (n=10), *tg* (n=7), and tg^{rol} (n=7) Purkinje cells. PF-EPSC peak amplitudes increased almost linearly with increments of stimulation intensity in wt and mutant mice.

B. Traces of PF-EPSC from wt (left), *tg* (middle), and tg^{rol} (right) Purkinje cells. Each trace is an average of ten current recordings in response to stimulation at 10V.

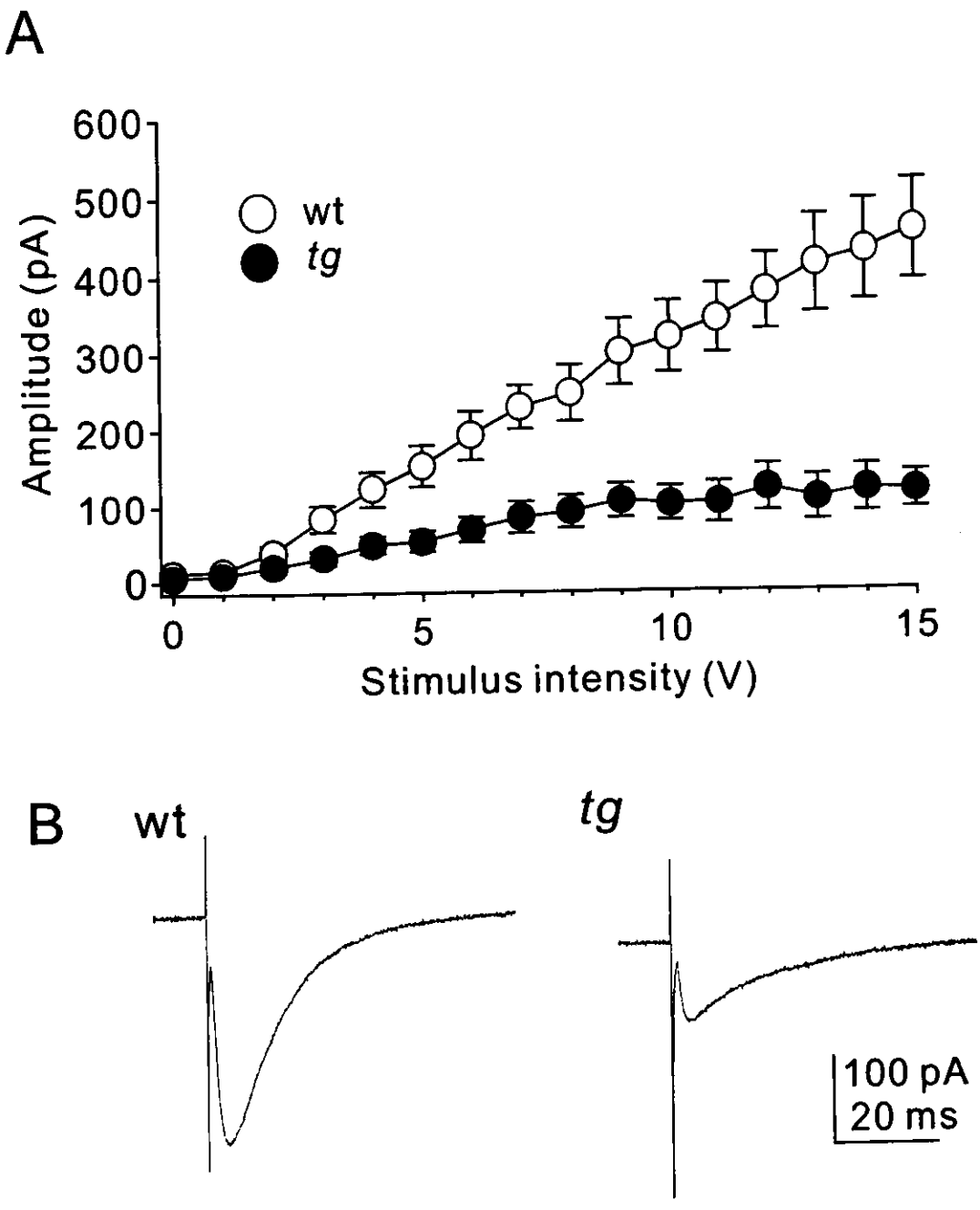
A
600
500
400
300
200
100
0
Amplitude (pA)
wt
tg
0
5
10
15
Stimulus intensity (V)
B
wt
tg
100 pA
20 ms

Fig.2.

Fig. 2. PF-PC synaptic transmission in ataxic *tg* mice

A. The stimulation intensity-PF-EPSC peak amplitude relationship, as in Fig. 1A, of wild-type and ataxic *tg* mice at P28-35. Averaged peak amplitudes were shown for wt (n=8) and *tg* (n=10) Purkinje cells.

B. Traces of PF-EPSC from wt (left) and *tg* (right) Purkinje cells. Each trace is an average of ten current recordings in response to stimulation at 10V.

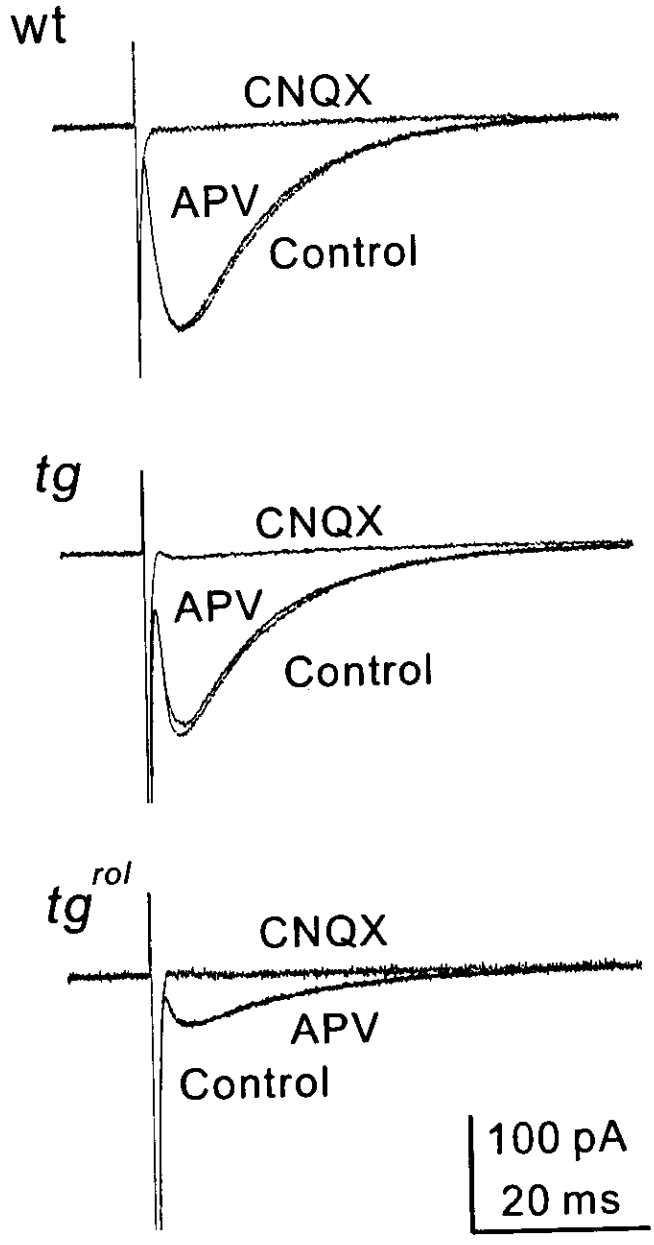
wt
CNQX
APV
Control
tg
CNQX
APV
Control
tg rol
CNQX
APV
Control
100 pA
20 ms

Fig.3.

Fig. 3. Effects of glutamate receptor antagonists on PF-EPSC

PF-EPSC traces of wt (top), *tg* (middle), and tg^{rol} (bottom) before and after application of APV or CNQX. PF-EPSCs were not affected by APV, but almost completely blocked by CNQX.

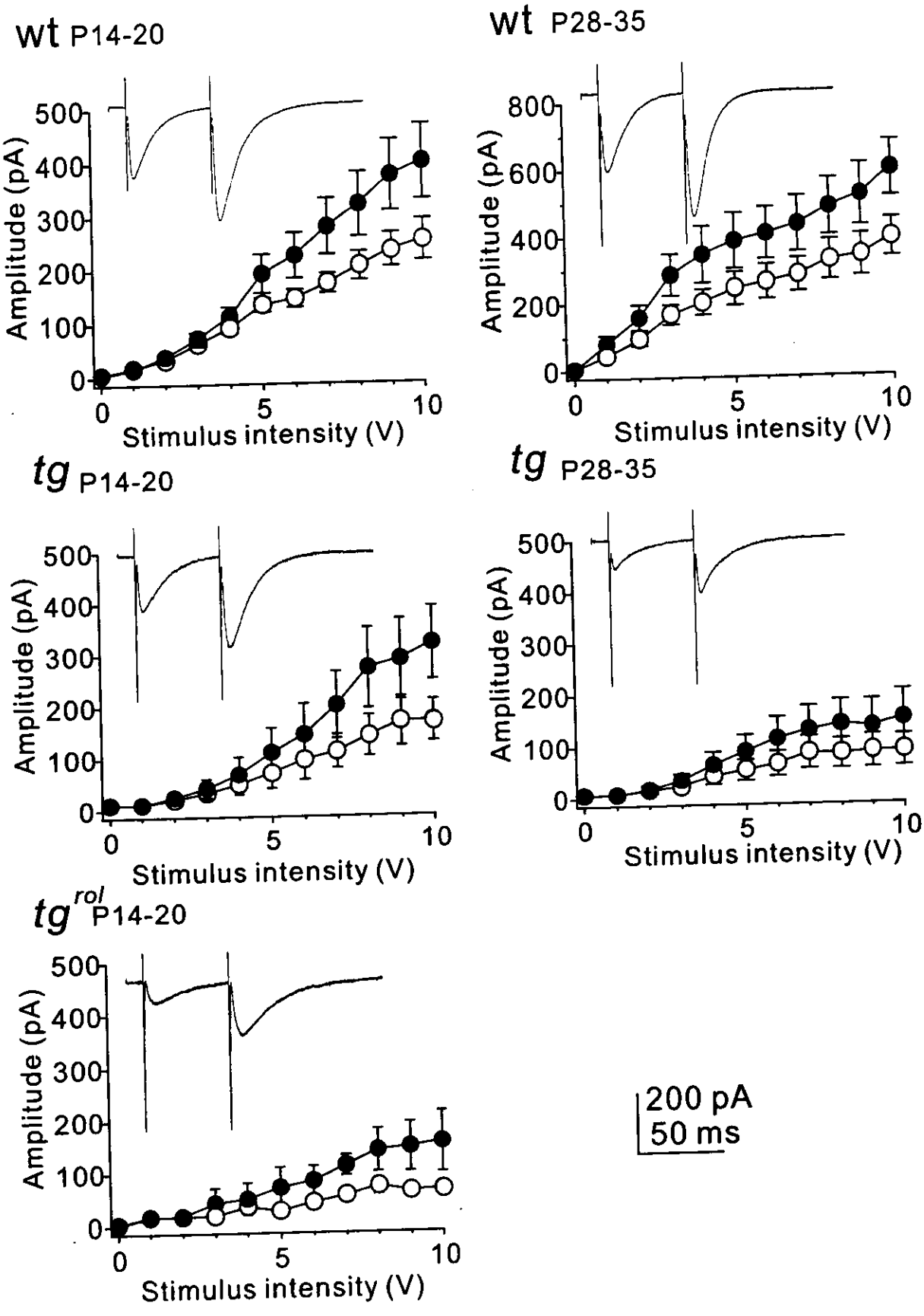
wt P14-20
Amplitude (pA)
500
400
300
200
100
0
0
5
10
Stimulus intensity (V)
wt P28-35
Amplitude (pA)
800
600
400
200
0
0
5
10
Stimulus intensity (V)
tg P14-20
Amplitude (pA)
500
400
300
200
100
0
0
5
10
Stimulus intensity (V)
tg P28-35
Amplitude (pA)
500
400
300
200
100
0
0
5
10
Stimulus intensity (V)
tg rol P14-20
Amplitude (pA)
500
400
300
200
100
0
0
5
10
Stimulus intensity (V)
200 pA
50 ms

Fig.4.

Fig. 4. Paired-pulse facilitation in PF-EPSC

The stimulation intensity-PF-EPSC peak amplitude relations for paired pulse stimulation (interval 50 ms) of wt and mutants. The mean peak amplitudes to the first stimulation (blank circles) and to the second stimulation (filled circles) were obtained from 10 measurements. Calibration is common for all traces. The insets show typical current traces (average of 10 recordings).

A
Normalized amplitude (%)
250
200
150
100
50
0
P14-20
*
wt
tg
tg^rol
B
Normalized amplitude (%)
200
150
100
50
0
P28-35
wt
tg

Fig.5.

Fig. 5. Enhanced paired-pulse facilitation in *tg^{rol}*

A. Averaged paired-pulse ratio (the second EPSC/ the first EPSC) of wt (n=10), *tg* (n=10), and *tg^{rol}* (n=10) Purkinje cells at P14-20.

B. Paired-pulse ratio of wt (n=10) and *tg* (n=10) Purkinje cells at P28-35.

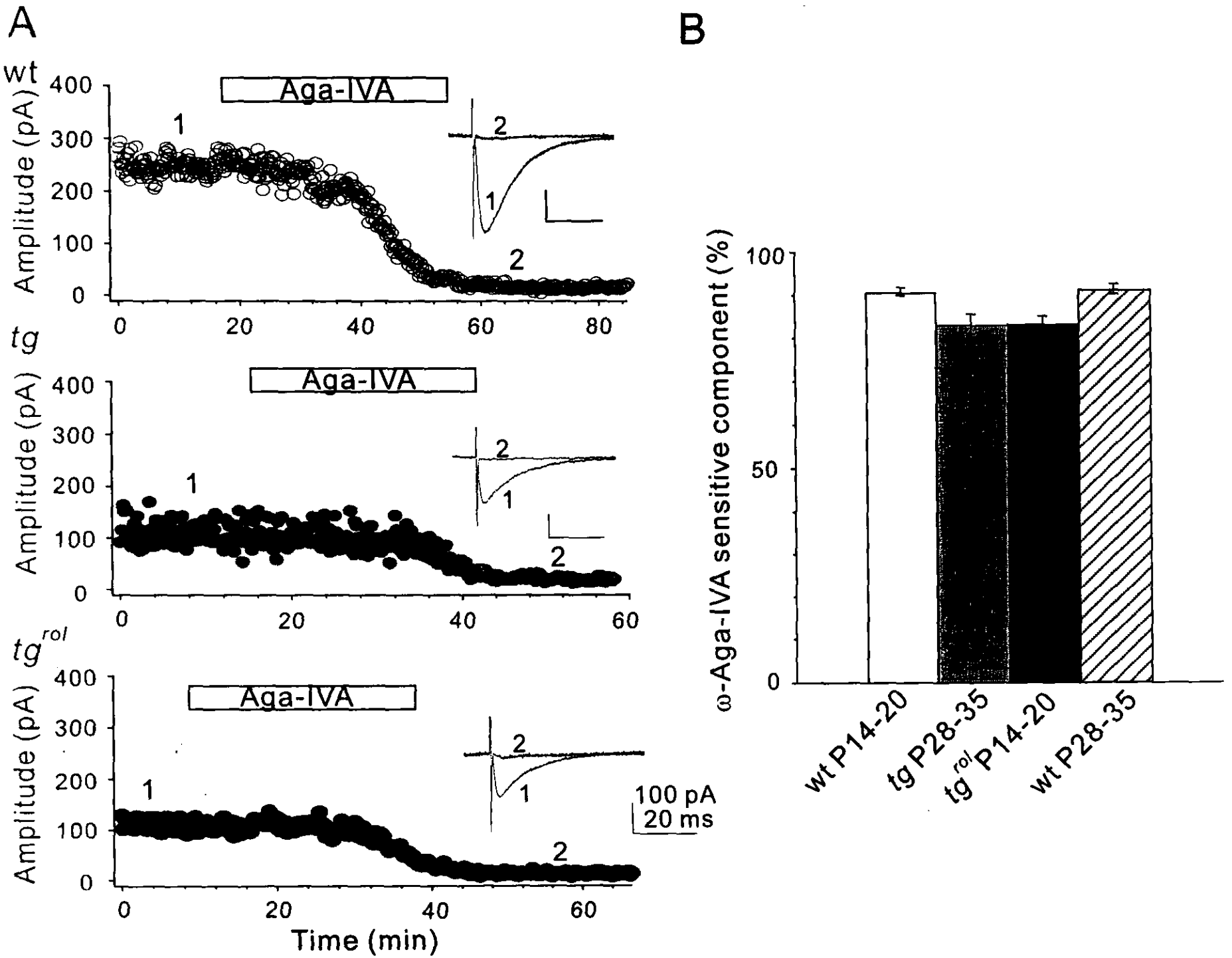
A
wt
Aga-IVA
Amplitude (pA)
400
300
200
100
0
0
20
40
60
80
1
2
tg
Aga-IVA
Amplitude (pA)
400
300
200
100
0
0
20
40
60
1
2
tg rol
Aga-IVA
Amplitude (pA)
400
300
200
100
0
0
20
40
60
Time (min)
1
2
100 pA
20 ms
B
ω-Aga-IVA sensitive component (%)
100
50
0
wt P14-20
tg P28-35
tg rol P14-20
wt P28-35

Fig.6.

Fig. 6. ω-AgaIVA sensitivity of PF-EPSC

A. Time course of the peak PF-EPSC amplitude in response to application of 0.2 μM ω-Aga-IVA (white bar). The insets show current traces at the time indicated by the numbers. Each trace is an average of ten recordings.

B. The ω-Aga-IVA-sensitive component (mean ± SEM) of PF-EPSC of wt, *tg*, and tg^{rol} from 3-5 measurements.

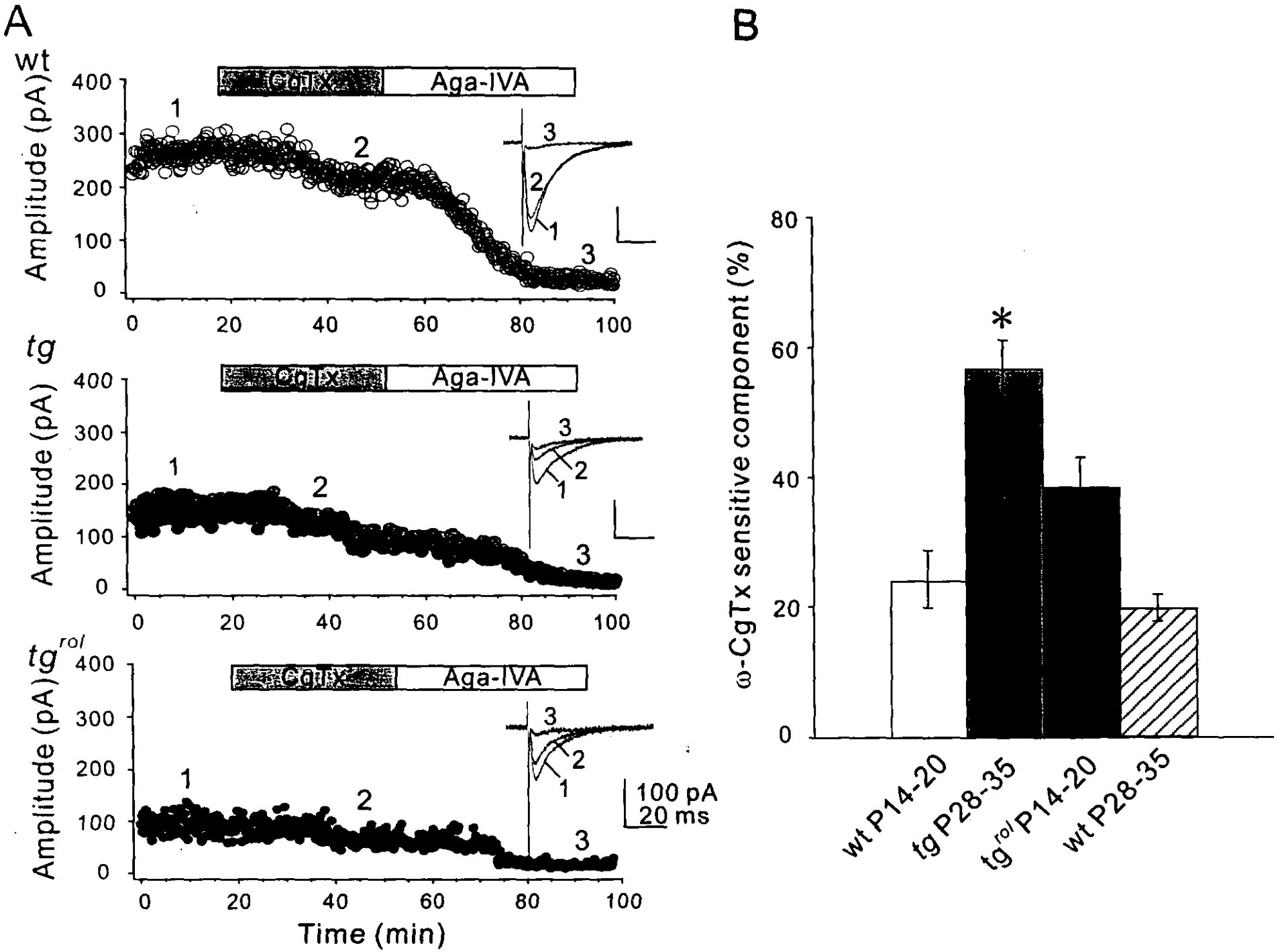
A
wt
tg
tg rol
Amplitude (pA)
CgTx
Aga-IVA
1
2
3
100 pA
20 ms
Time (min)
B
ω-CgTx sensitive component (%)
*
wt P14-20
tg P28-35
tg rol P14-20
wt P28-35

Fig. 7.

Fig. 7. ω-CgTx sensitivity of PF-EPSC

A. Time course of the peak PF-EPSC amplitude in response to application of 3 μM ω-CgTx and 0.2 μM ω-Aga-IVA. The insets show current traces at the time indicated by the numbers. Each trace is an average of ten recordings.

B. The ω-CgTx sensitive components (mean ± SEM) of CF-EPSC of wt, *tg*, and tg^{rol} from 3-6 measurements.

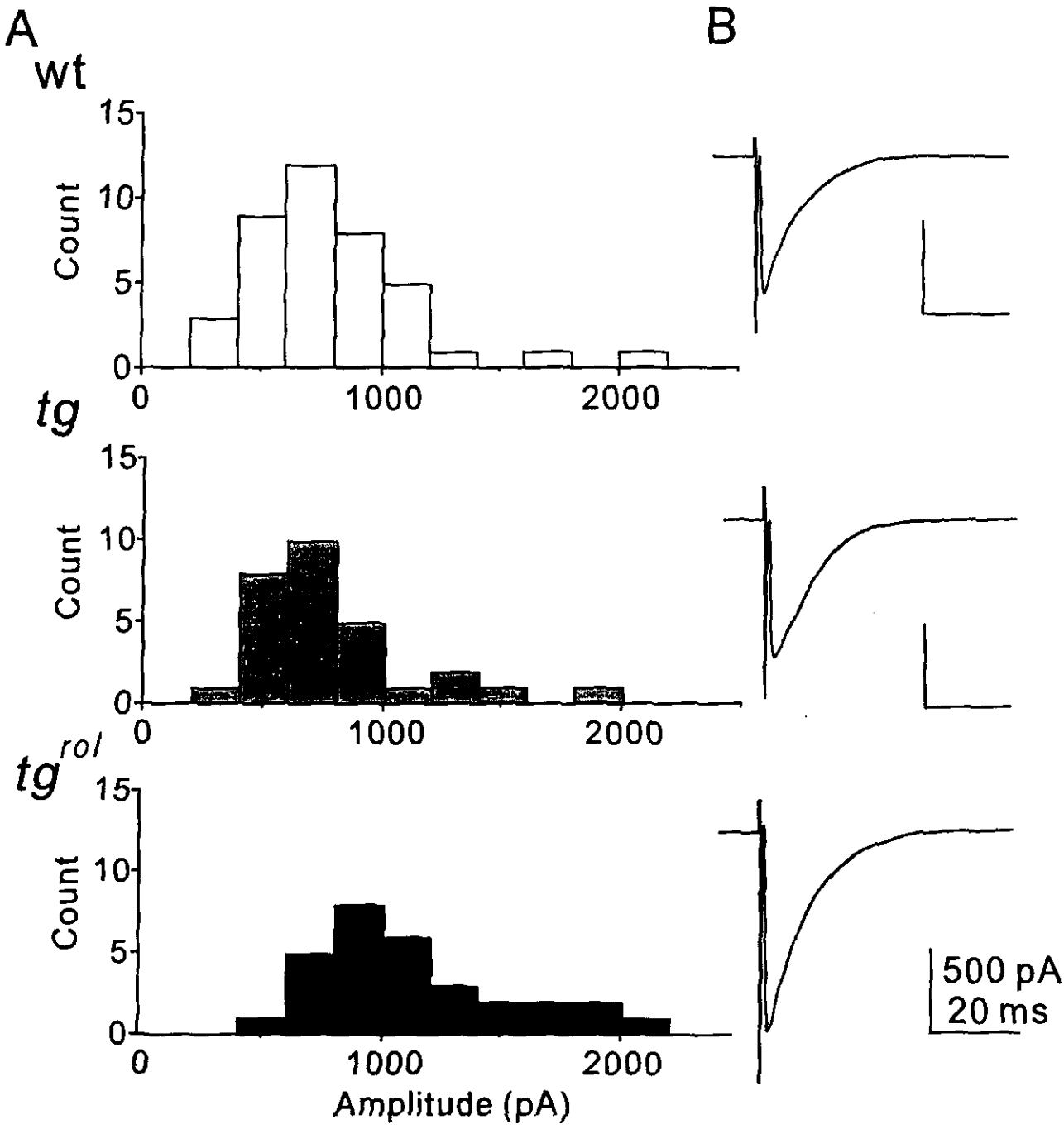
A
B
wt
tg
tg rol
Count
15
10
5
0
0
1000
2000
500 pA
20 ms
Amplitude (pA)
C
1500
1000
500
0
Amplitude (pA)
*
wt
tg
tg rol

Fig. 8.

Fig. 8. CF-PC synaptic transmission in mutant mice

A. The distribution of the CF-EPSC peak amplitude of wt (n=40), *tg* (n=30), and tg^{rol} (n=31) Purkinje cells at P 14-20. All Purkinje cells were monoinnervated.

B. Typical traces of CF-EPSC from wt (top), *tg* (middle), and tg^{rol} (bottom) Purkinje cells at P14-20. Three to five traces were averaged.

C. Mean peak amplitudes of CF-EPSC of wt, *tg*, and tg^{rol} at P14-20. Values are presented as mean ± SEM. $*p < 0.05$

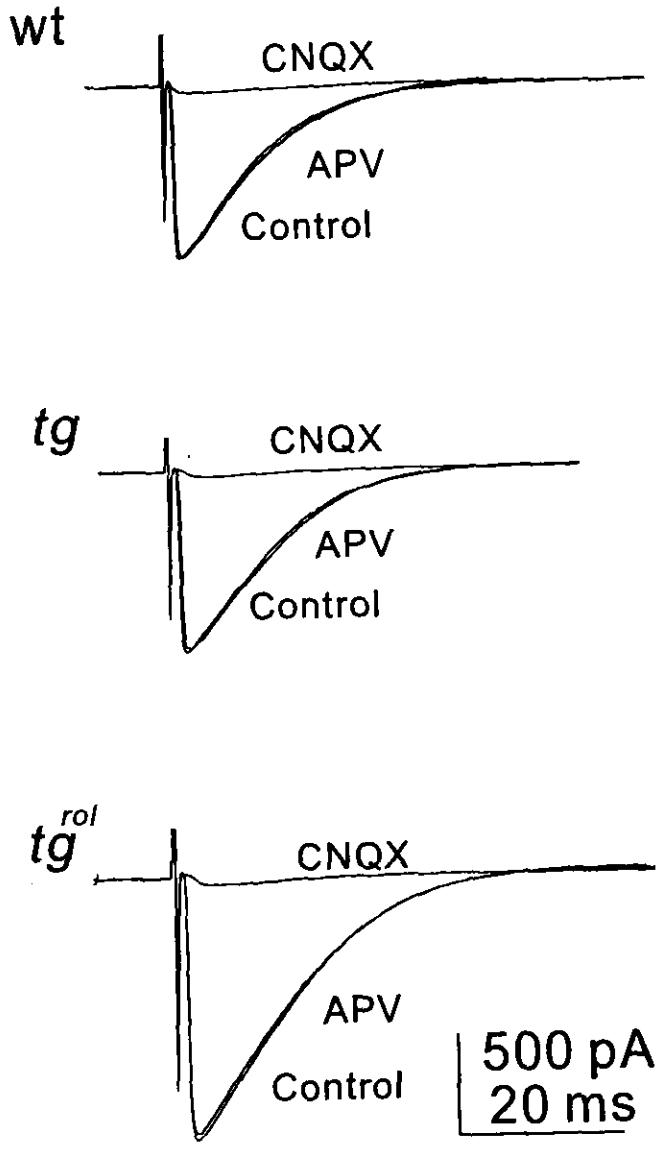
wt
CNQX
APV
Control
tg
CNQX
APV
Control
tg rol
CNQX
APV
Control
500 pA
20 ms

Fig. 9.

Fig. 9. Effects of glutamate receptor antagonists on CF-EPSC

CF-EPSC traces of wt (top), *tg* (middle), and tg^{rnl} (bottom) before and after application of APV or CNQX. CF-EPSCs were not affected by APV, but almost completely blocked by CNQX.

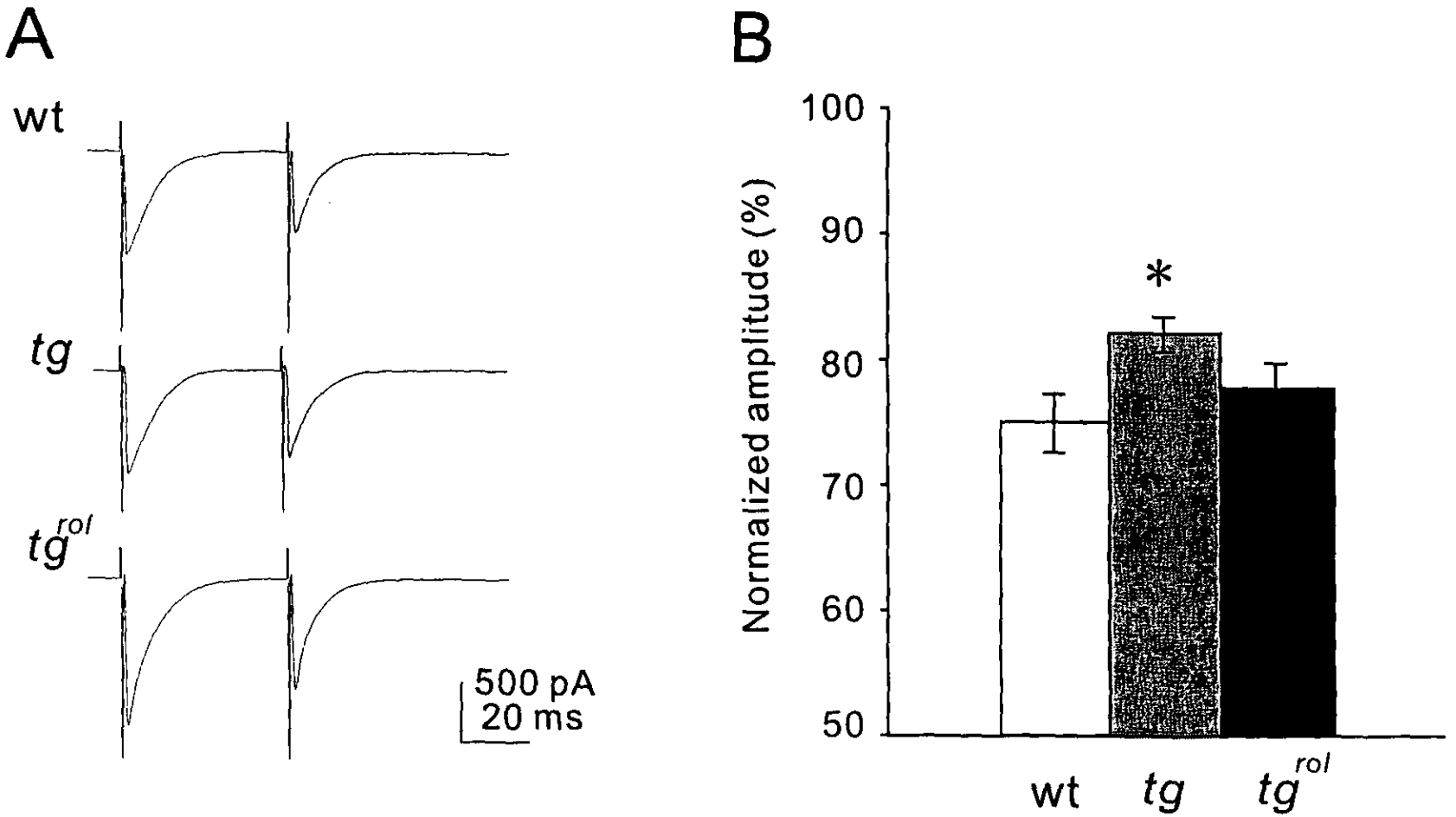
A
wt
tg
tg^rol
500 pA
20 ms
B
Normalized amplitude (%)
100
90
80
70
60
50
*
wt
tg
tg^rol

Fig. 10.

Fig. 10. Paired-pulse depression in CF-EPSC

A. CF-EPSCs to pairs of stimuli separated by 50 ms in monoinnervated Purkinje cells of wt (n=17), *tg* (n=10), and *tg*^{rol} (n=10) at P14-20. Three to five traces were averaged.

B. Paired-pulse ratios (the second EPSC / the first EPSC, mean ± SEM) of wt (open bar, n=17), *tg* (gray bar, n=10), and *tg*^{rol} (filled bar, n=10). Note that the value of *tg* is larger than wt or *tg*^{rol} (*$p < 0.05$).

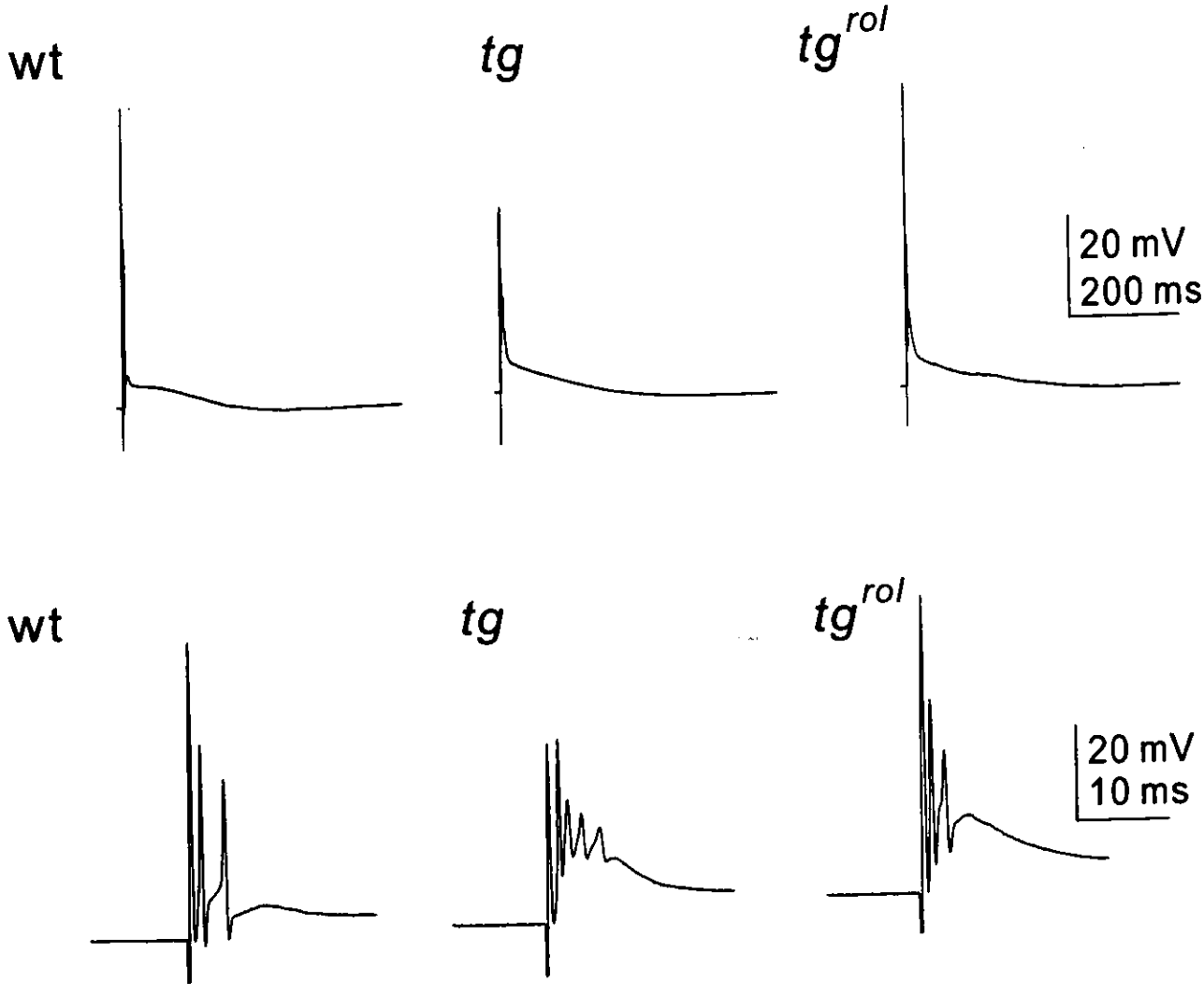

Fig.11.

Fig. 11. Complex spike generation by CF stimulation

A. Complex spikes produced by activation of CFs in wt, *tg* and *tg*^{rol} Purkinje cells.

B. Expanded traces of those in A.

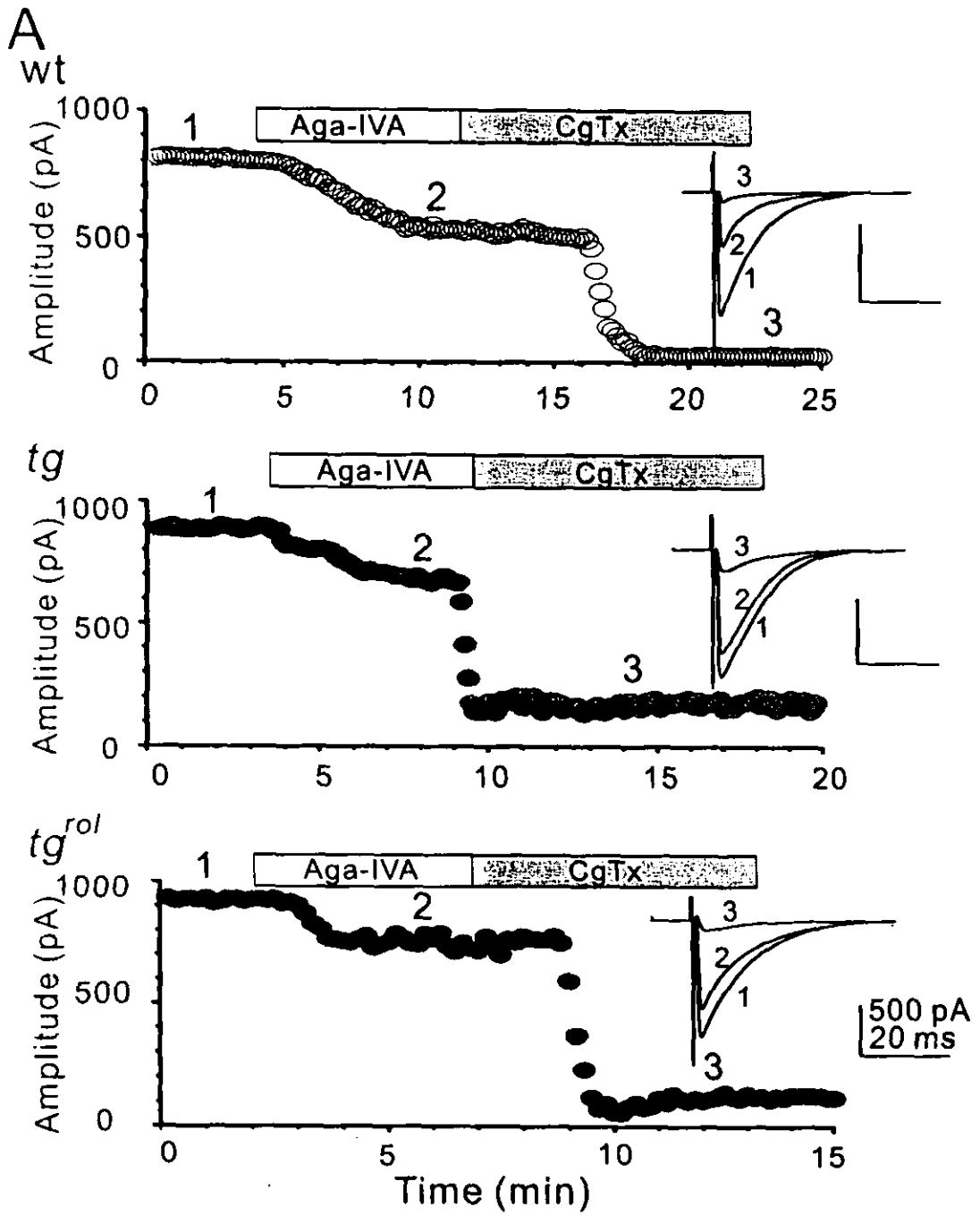
A
wt
Aga-IVA
CgTx
Amplitude (pA)
1000
500
0
0
5
10
15
20
25
1
2
3
tg
Aga-IVA
CgTx
Amplitude (pA)
1000
500
0
0
5
10
15
20
1
2
3
tg rol
Aga-IVA
CgTx
Amplitude (pA)
1000
500
0
0
5
10
15
1
2
3
500 pA
20 ms
Time (min)

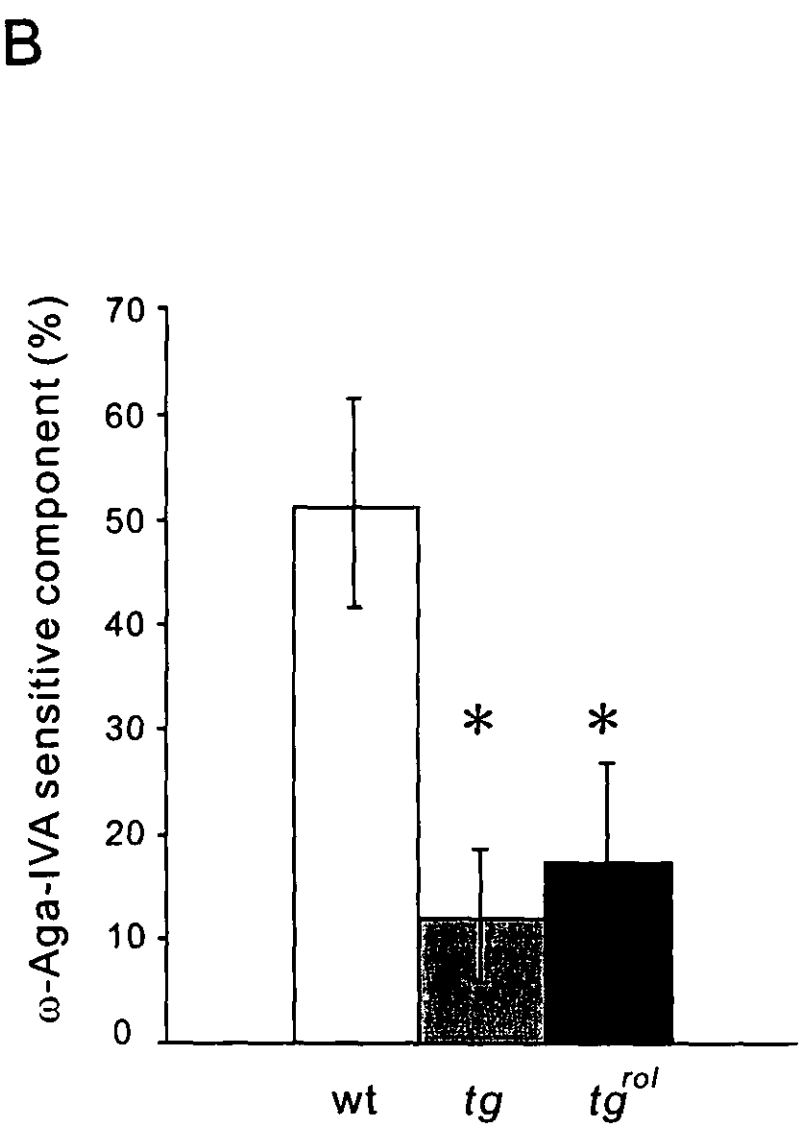
B
ω-Aga-IVA sensitive component (%)
70
60
50
40
30
20
10
0
*
*
wt
tg
tg rol

Fig. 12.

Fig. 12. ω-Aga-IVA sensitivity of CF-EPSC

A. Time course of the peak CF-EPSC amplitude in response to application of 0.2μM ω-Aga-IVA (white bar) and 3 μM ω-CgTx (gray bar). The insets show current traces at the time indicated by the numbers. Each trace is an average of five recordings.

B. ω-Aga-IVA sensitive components (mean ± SEM) of CF-EPSC of wt, *tg*, and tg^{rol} from 3-6 measurements.

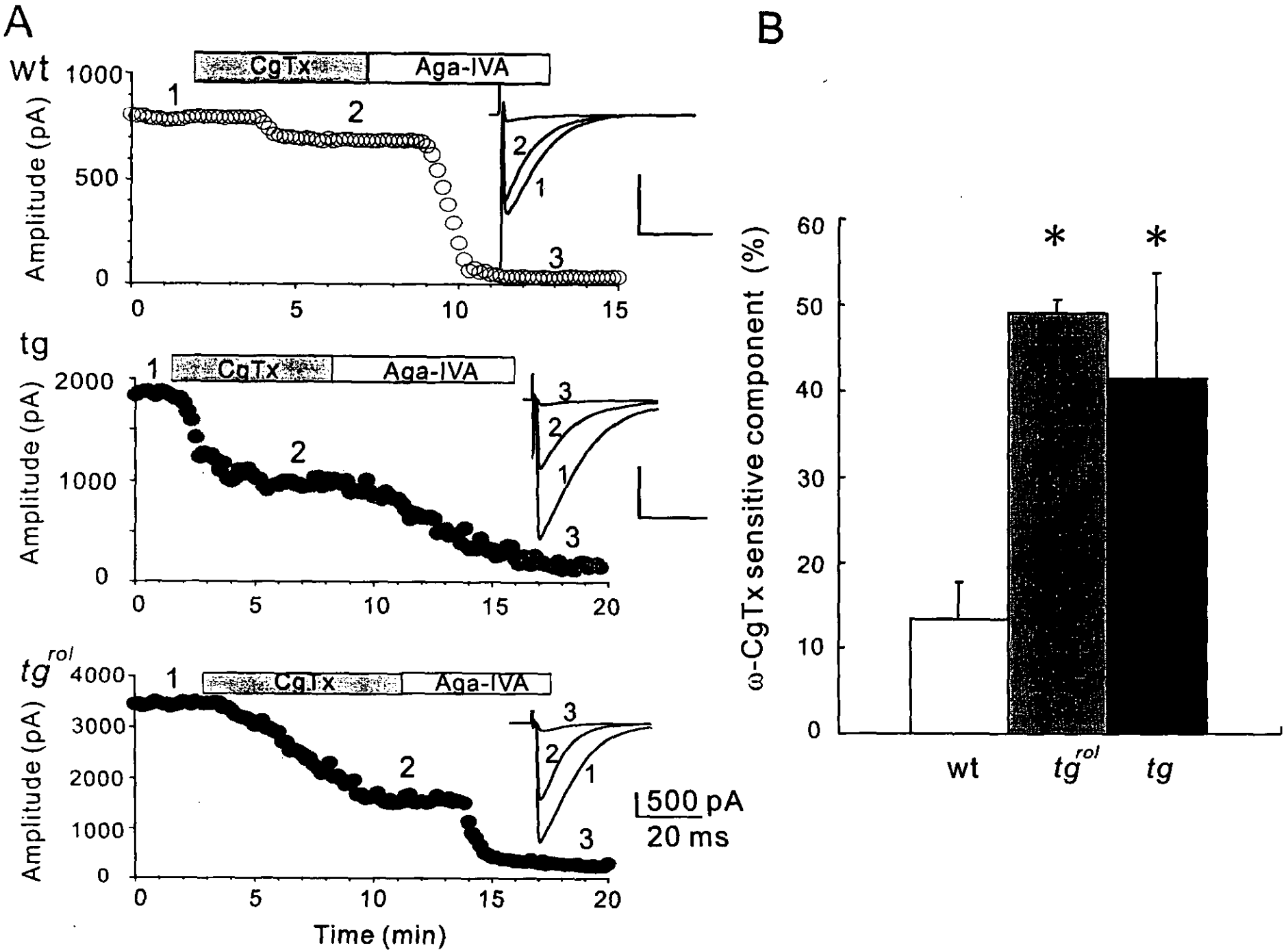
A
wt
CgTx
Aga-IVA
Amplitude (pA)
1000
500
0
1
2
3
0
5
10
15
tg
2000
1000
0
20
tg^{rol}
4000
3000
2000
1000
Time (min)
500 pA
20 ms
B
ω-CgTx sensitive component (%)
60
50
40
30
20
10
0
*
*
wt
tg^{rol}
tg

Fig. 13.

Fig. 13. ω-CgTx sensitivity of CF-EPSC

A. Time course of the peak CF-EPSC amplitude in response to application of 3 μM ω-CgTx (gray bar) and 0.2μM ω-Aga-IVA (white bar). The insets show current traces at the time indicated by the numbers. Each trace is an average of five recordings.

B. ω-CgTx sensitive components (mean ± SEM) of the CF-EPSC of wt, *tg*, and tg^{rol} from 3-6 measurements.

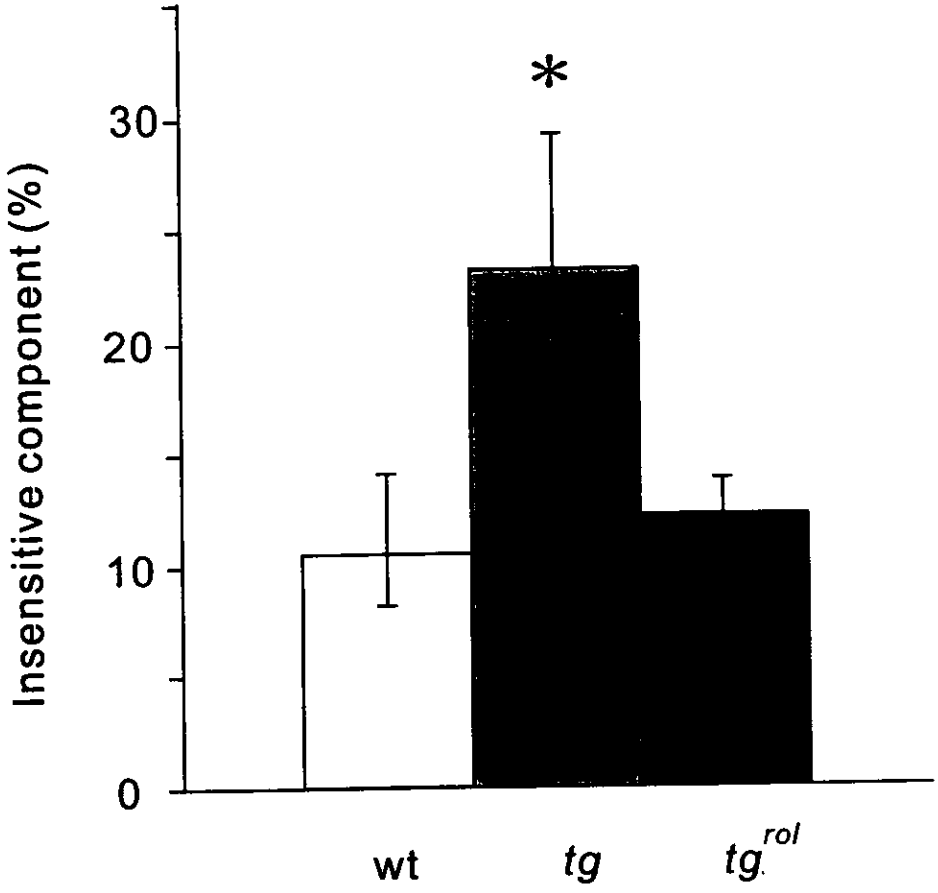

Fig.14.

Fig. 14. CF-EPSC component insensitive to ω-Aga-IVA and ω-CgTx

The remaining component after application of ω-Aga-IVA and ω-CgTx from 6-8 measurements ($^*p < 0.05$).

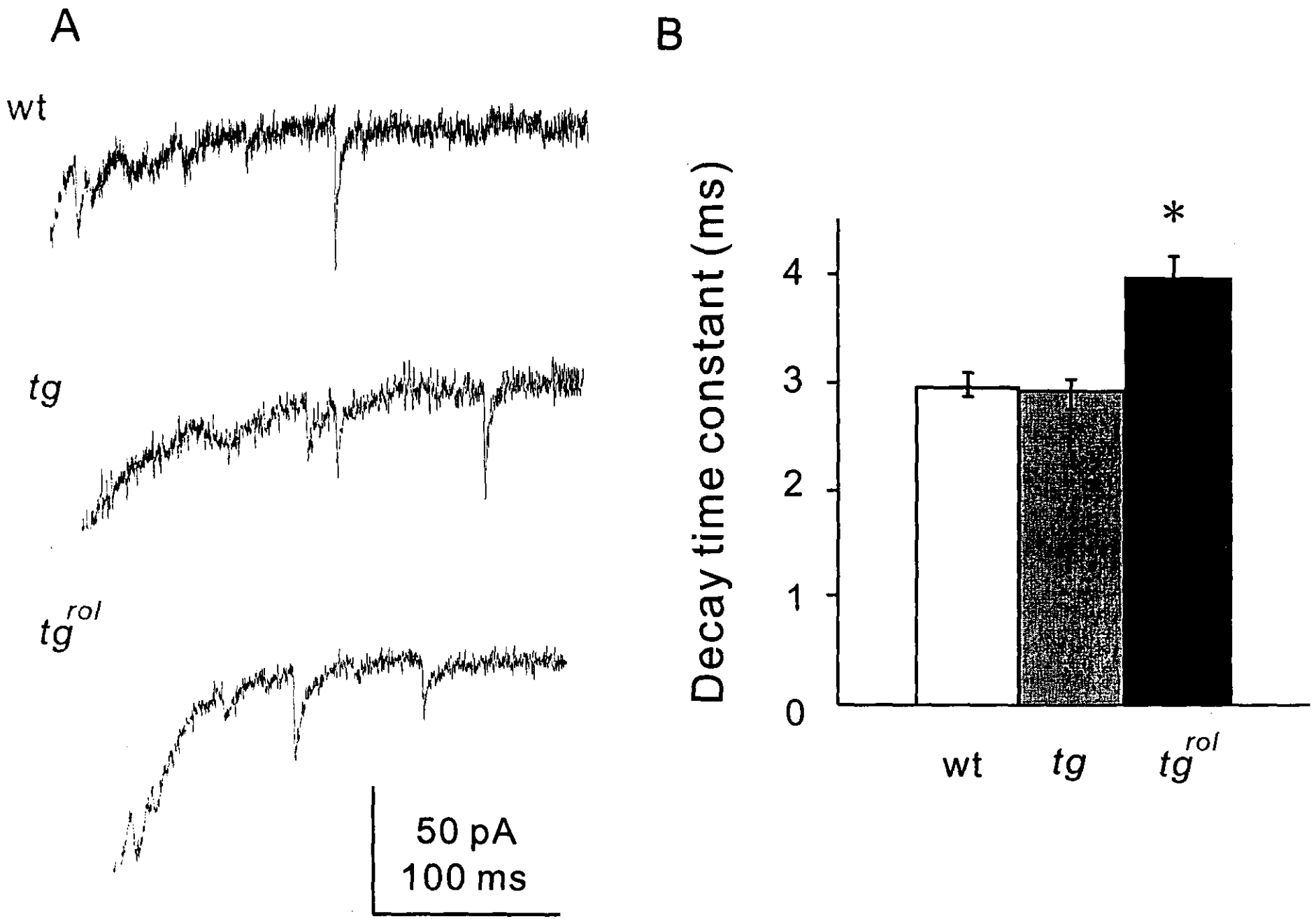
A
wt
tg
tg rol
50 pA
100 ms
B
Decay time constant (ms)
0
1
2
3
4
*
wt
tg
tg rol

Fig. 15.

Fig. 15. Miniature CF-EPSCs in Sr^{2+} solution

A. Traces of miniature CF-EPSCs in response to CF stimulation, recorded from wt (top), *tg* (middle), and tg^{rol} (bottom) Purkinje cells. The peak of CF-EPSC was cropped to illustrate asynchronous quantal events in the tail.

B. The decay time constant (mean ± SEM) of miniature CF-EPSCs of wt, *tg*, and tg^{rol}. 190-270 events were averaged.

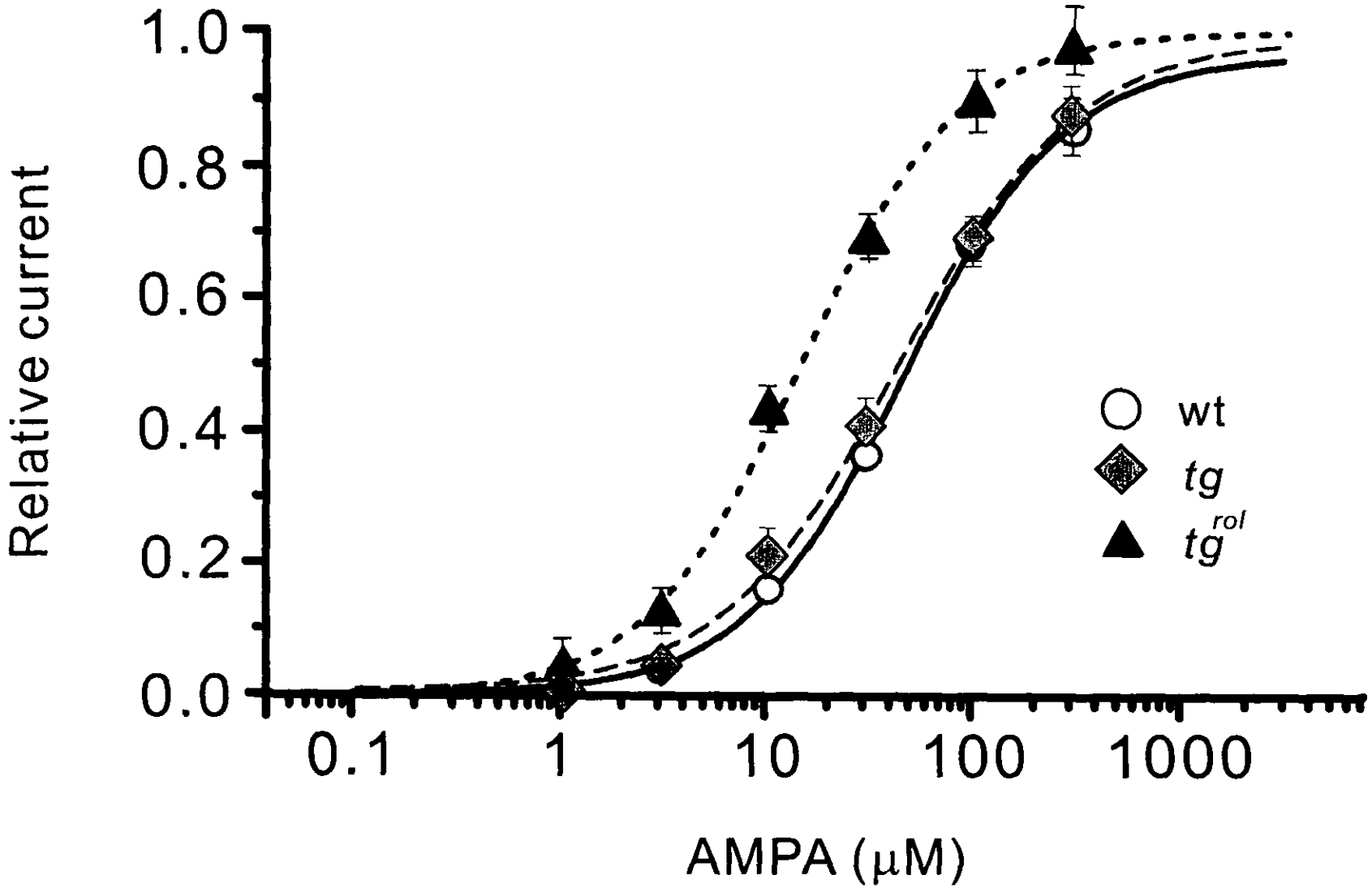
Relative current
1.0
0.8
0.6
0.4
0.2
0.0
0.1
1
10
100
1000
AMPA (μM)
wt
tg
tg rol

Fig.16.

Fig. 16. AMPA sensitivity of dissociated Purkinje cells

The AMPA concentration-response curves of wt, *tg*, and tg^{rol}. Data from each cell were normalized to the Imax value obtained from the Hill equation. Values are presented as mean ± SEM.

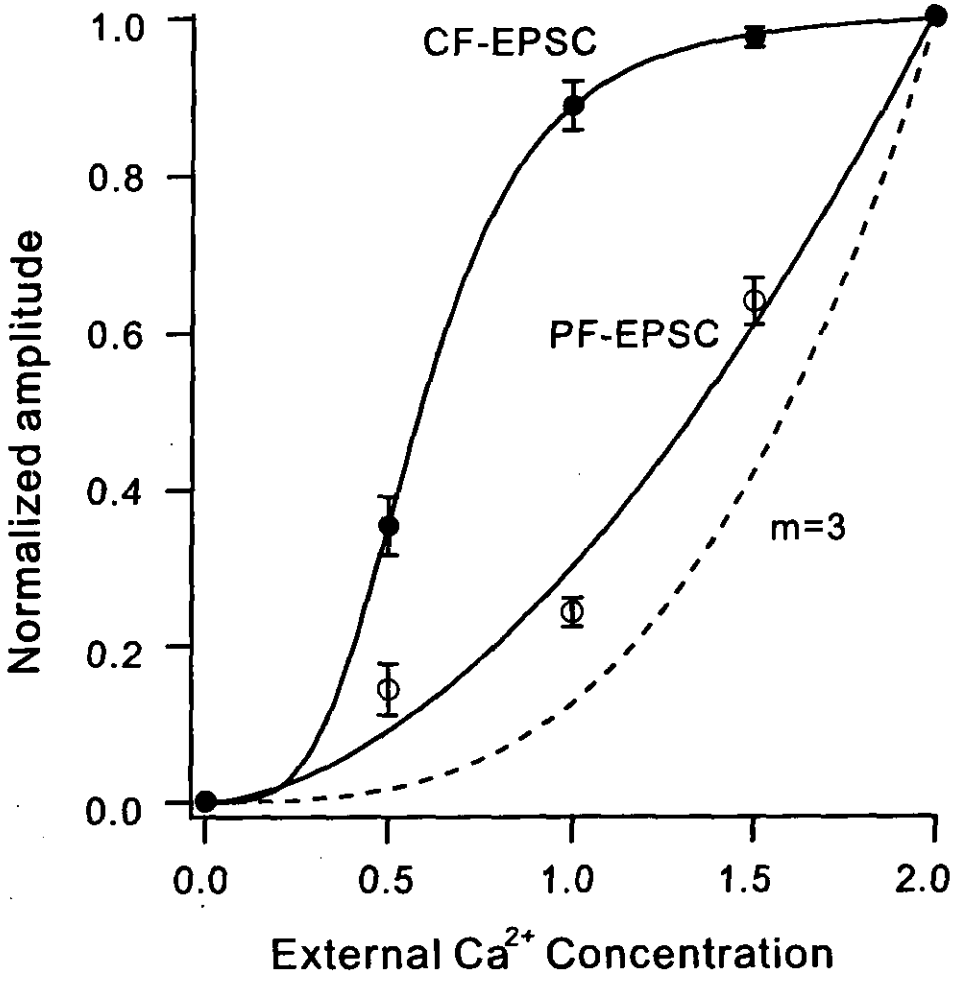
1.0
0.8
0.6
0.4
0.2
0.0
Normalized amplitude
CF-EPSC
PF-EPSC
m=3
0.0
0.5
1.0
1.5
2.0
External Ca2+ Concentration

Fig.17.

Figure 17. Effect of lowering the external Ca^{2+} concentration on PF-and CF-EPSC amplitude

Peak EPSC amplitude was plotted as a function of the external Ca^{2+} concentration. The current amplitude was normalized to that at 2 mM external Ca^{2+}. The normalized PF-EPSC amplitude was fit by the power relation, $y = kx^m$, where $k = 0.3$ and $m = 1.7$. The relation of the third power relation was shown for comparison (dotted line). The normalized CF-EPSC amplitude was fit by the Hill's equation, $y = k/(1+(d/x)^m)$, where $k = 1.0$, $m = 3.8$, and the relative half-saturation concentration $d = 0.29$.

Table 1. Basic properties of PF-EPSCs in mutant mice

Mice (P14-20)	Amplitude (pA)	Decay time constant (ms)	10 %-90 % Rise time (ms)	Paired-pulse ratio (%)
wt	272.6 ± 30.4 (14)	12.1 ± 1.3 (14)	1.82 ± 0.16 (10)	165.3 ± 7.9 (11)
tg	*168.3 ± 26.4 (14)	12.0 ± 0.8 (14)	2.26 ± 0.21 (10)	181.9 ± 6.0 (10)
tg^{rvl}	*79.6 ± 11.7 (10)	12.9 ± 1.6 (10)	2.44 ± 0.34 (10)	*212.8 ± 18.7 (10)

Mice (P28-32)	Amplitude (pA)	Decay time constant (ms)	10 %-90 % Rise time (ms)	Paired-pulse ratio (%)
wt	319.4 ± 21.3 (10)	12.4 ± 1.4 (10)	2.08 ± 0.29 (10)	158.9 ± 4.5 (10)
tg	88.76 ± 46.3 (10)	13.0 ± 2.3 (10)	2.22 ± 0.52 (10)	159.6 ± 9.7 (10)

PF-EPSCs were evoked by 10 V stimulation. All data were expressed as mean ± SEM. Numbers of recorded Purkinje cells were shown in the parentheses. The decay time constant was obtained by fitting the EPSC decay with a single exponential. Paired-pulse ratio is second EPSC/ first EPSC. Interpulse interval was 50 ms. * $p < 0.05$.

Table 2. PF-EPSC fractions remaining after application of Ca^{2+} channel-blocking toxins

Toxins applied	ω-Aga-IVA (*a*)	ω-CgTx (*b*)	ω-Aga-IVA + ω-CgTx (*c*)	*a* + *b* + *c*
wt	0.09 ± 0.01 (0.55)	0.76 ± 0.04 (0.09)	0.08 ± 0.01 (0.43)	(1.07)
tg	0.17 ± 0.02 (0.45)	0.43 ± 0.04 (0.24)	0.18 ± 0.05 (0.56)	(1.25)
tg^{rol}	0.17 ± 0.02 (0.44)	0.61 ± 0.05 (0.15)	0.23 ±0.03 (0.61)	(1.20)

Each value represents mean ± SEM of three or four measurements. Numbers in parentheses (*a-c*) are the estimated fractions of Ca^{2+} channel subtype mediating synaptic transmission, assuming a third power relation between presynaptic Ca^{2+} concentration and postsynaptic response amplitude.

Table 3. Basic properties of CF-EPSCs in mutant mice

Mice (P14-20)	Amplitude (pA)	Decay time constant (ms)	10 %-90 % Rise time (ms)	Paired-pulse ratio (%)
wt	787.7 ± 55.9 (40)	11.6 ± 0.5 (39)	0.41 ± 0.02 (14)	75.0 ± 2.3 (17)
tg	793.2± 61.4 (30)	11.1 ± 0.6 (14)	0.39 ± 0.04 (10)	*82.1± 1.4 (10)
tg^{pl}	*1149 ± 67.5 (31)	*15.7 ± 1.0 (10)	0.39 ± 0.02 (10)	77.6 ± 2.2 (10)

Mice (P28-32)	Amplitude (pA)	Decay time constant (ms)	10 %-90 % Rise time (ms)	Paired-pulse ratio (%)
wt	841.1 ± 52.5 (10)	12.7 ± 0.6 (6)	0.34 ± 0.01 (6)	77.2 ± 1.8 (10)
tg	841.9 ± 91.7 (10)	12.3 ± 1.5 (9)	0.48 ± 0.04 (10)	*87.2 ± 1.1 (10)

All data were expressed as mean ± SEM. Numbers of the recorded Purkinje cells were shown in the parentheses. The decay time constant was obtained by fitting the EPSC decay with a single exponential. Paired-pulse ratio is second EPSC/ first EPSC. Interpulse interval was 50 ms for CF-EPSCs. * $p < 0.05$.

Table 4. CF-PC percentages remaining after application of Ca^{2+} channel-blocking toxins.

Toxins applied	ω-Aga-IVA (a)	ω-CgTx (b)	ω-Aga-IVA + ω-CgTx (c)	a+b+c
wt	45.8 ± 7.4 (23)	83.1 ± 3.3 (6)	10.6 ± 3.4 (47)	(76)
tg	87.7 ± 6.4 (43)	50.9 ± 1.5 (20)	23.3 ± 6.5 (62)	(87)
tg^{rol}	82.8 ± 9.7 (62)	68.8 ± 6.4 (12)	12.2 ±1.6 (72)	(90)

Each value represents mean (± SEM) of three or four measurements.

Numbers in parentheses (a-c) are the estimated percentages of Ca^{2+} channel subtype mediating synaptic transmission, assuming a third power relation between presynaptic Ca^{2+} concentration and postsynaptic response amplitude.

Table 5. CF-EPSC fractions remaining after application of Ca^{2+} channel-blocking toxins, fit using the Hill's equation.

Toxins applied	ω-Aga-IVA (*a*)	ω-CgTx (*b*)	ω-Aga-IVA + ω-CgTx (*c*)	*a* + *b* + *c*
wt	0.46± 0.07 (0.46)	0.83 ± 0.03 (0.18)	0.11 ± 0.03 (0.34)	(0.98)
tg	0.88 ± 0.06 (0.18)	0.51 ± 0.02 (0.43)	0.24± 0.07 (0.33)	(0.94)
tg^{rol}	0.83 ± 0.10 (0.23)	0.69 ± 0.06 (0.33)	0.12 ± 0.02 (0.35)	(0.91)

Each value represents mean (± SEM) of three or four cells.

Numbers in parentheses (*a-c*) are the estimated fractions of Ca^{2+} channel subtype mediating synaptic transmission, using the Hill's equation between presynaptic Ca^{2+} concentration and postsynaptic response amplitude.